Low Complexity Power-efficient Waveform Design for RIS-aided ISAC

Prabhat Raj Gautam, *Member, IEEE,* and Julie A. McCann

***Abstract*—We consider an integrated sensing and communication (ISAC) system in which a base station (BS) communicates with several users with the help of a reconfigurable intelligent surface (RIS), sensing targets at the same time. We design a power-efficient ISAC scheme that limits communication and sensing power by maintaining a minimum required signal-to-interference-and-noise ratio (SINR) at the communication user and a minimum required received sensing SINR. The sensing signal is implemented by minimizing the difference between the beampattern of the ISAC signal and the desired beampattern. Unlike the existing state-of-the-art power-efficient ISAC waveforms, the communication signal is also included in the design of the sensing signal to limit its impact on sensing performance. We obtain the communication signal by designing a precoder, that meets the minimum SINR constraint with minimum power, jointly with the passive beamforming at the RIS. To this end, we propose two separate algorithms, *viz.*, one based on alternating optimization, which alternately optimizes passive beamforming and transmit precoder, and the second one based on manifold optimization in which we optimize passive beamforming first, followed by the optimization of the transmit precoder. A low-complexity algorithm based on the first-order optimization condition is employed to produce a sensing signal, which is later projected onto the null space of the communication channel to nullify its effect on the communication performance. The power of the dedicated sensing signal is adjusted to meet the individual sensing SINR constraints at the receiver, which helps reduce the total transmit power. Simulations demonstrate that the proposed algorithms achieve improved communication and sensing performance, with up to a 2 dB reduction in transmit communication power and up to a 4 dB reduction in normalized beampattern along angles outside the target location, compared to the existing state-of-the-art solution.**

***Index Terms*—Integrated sensing and communication (ISAC), power-efficient, waveform design, reconfigurable intelligent surface (RIS).**

I. Introduction

Future wireless communication technologies conceive of incorporating communication and radar sensing into a single system known as Integrated Sensing and Communication (ISAC). ISAC allows the sharing of spectrum, hardware, and signal processing resources between the communication and sensing applications, lowering implementation costs while promoting spectrum and energy efficiency. The simplest way to make ISAC realizable is by making radar sensing and communication use the same spectrum by opportunistic spectrum sharing [1], [2] or transmitting in different time instants [3]. These approaches, while innocuous, do not make use of the available resources in an efficient way. The techniques in [4]–[7] use null space projection to allow radar and communication systems to coexist while sharing the same spectrum and time resources.

Depending on whether we prioritize sensing or communication in design, the ISAC waveform design can be categorized as sensing-centric design or communication-centric design [8]. On the other hand, the joint design approach prioritizes communication and sensing by developing a waveform that meets both communication and sensing performance targets. The sensing-centric design uses the radar waveform with communication data embedded on the radar signal [8], [9]. In contrast, the communication-centric design employs the conventional communication waveform for radar sensing [8]. The various techniques used to encode communication data onto the radar signal are pulse interval modulation [10], controlling radar spatial side-lobes [11], [12], index modulation [13]–[15], phase shift keying (PSK) [16]–[18], spatial modulation [19] and carrier frequency modulation [20]. [21] introduces Orthogonal Frequency Division Multiplexing (OFDM), designed for simultaneous radar sensing and communication operations, and derives system parameterization for operation at 24 GHz that fulfills both requirements. In [22], design approaches based on classical phase-coded waveforms are proposed for simultaneous data transmission and radar sensing using OFDM.

The joint design route involves applying optimization methods to solve the problem that encapsulates sensing and communication performance [23], [24]. In [23], the communication beamformer is computed making sure that the obtained beampattern matches the sensing beampattern that meets communication performance requirements in a separated deployment of sensing and communication antennas. In contrast, the sensing beampattern is designed to meet communication SINR requirements for shared deployment of sensing and communication antennas in [23]. [24] proposes low complexity algorithms to design a waveform by performing weighted optimizations for a tradeoff between sensing and communication performance. Liu *et al.* [9] pose ISAC waveform design as a problem of optimizing communication and radar transmit precoding with the MIMO radar beampattern as performance metric, while satisfying SINR constraints at

Prabhat Raj Gautam is with the Department of Computing, Imperial College London, London, UK (e-mail: p.gautam@imperial.ac.uk).
Julie A McCann is with the Department of Computing, Imperial College London, London, UK (email: j.mccann@imperial.ac.uk).
This work was supported by the EPSRC through the Communications Hub for Empowering Distributed Cloud Computing Applications and Research (CHEDDAR) [grant numbers EP/X040518/1 and EP/Y037421/1].

each communication user. Cramér-Rao Lower Bound (CRLB) constrained to meet SINR at each communication user is used as an objective function to design the waveform in [8]. He *et al.* [25] propose to compute the communication precoder and sensing signal by maximizing communication energy efficiency of the system while guaranteeing the sensing performance in terms of radar illumination along individual target direction. In [26], waveform with tunable peak-to-average power ratio (PAPR) is designed by formulating a non-convex optimization problem that minimizes multi-user interference for communication, while enforcing similarity to a specified radar chirp signal. An RIS-aided bistatic ISAC system is proposed in [27] that optimizes RIS phase shifts, transmit covariance, and analog beamforming at the passive receiver to minimize interference from direct and indirect paths, thereby reducing the dynamic range at the sensing unit while maintaining communication and sensing performance.

In [28], a waveform is designed for a full duplex ISAC system in which communication downlink and uplink are happening simultaneously, along with the sensing of a target. The downlink ISAC transmit signal is jointly computed with uplink receive beamformers at the BS and the transmit power at the uplink users, with the objectives to minimize transmit power and maximize sum rate. Two sensing criteria, matching of the ISAC waveform beampattern with the desired beampattern and the maximization of the minimum weighted ISAC waveform beampattern gain, are adopted in [29] to optimize sensing performance while guaranteeing SINR requirements at the communication users. The authors consider two types of communication receivers in [29], which have and do not have the capability of canceling the interference from the *a-priori* known dedicated radar signals. Chen *et al.* [30] propose two waveforms for an RIS-aided ISAC, both of which use minimization of sensing beampattern matching error as the sensing performance criterion. As for communication performance, the maximization of weighted communication sum rate and the minimization of communication power with assured SINR performance for communication users are employed as optimization criteria. Yiu *et al*. emphasize robustness and security, synchronization issues, or movable-antenna-enabled airborne ISAC beamforming in [31]–[33]. Authors of [31] propose a robust optimization framework for an RIS-assisted autonomous aerial vehicle (AAV) ISAC system that jointly optimizes the AAV trajectory, RIS, and beamforming to maximize secrecy rate for communications while satisfying sensing constraints under imperfect eavesdropper's channel information. In [32], a movable-antenna-enabled ISAC system is presented for low-altitude vehicle system that jointly optimizes antenna positioning and beamforming to maximize communication SNR while satisfying sensing SNR constraint. Yiu *et al*. [33] propose a movable antenna-aided cooperative ISAC system that jointly accounts for time synchronization and channel state information (CSI) errors, optimizing antenna position, beamforming, and base station (BS) selection factor via constrained deep reinforcement learning to minimize power while maintaining robust communication and sensing performance.

The ISAC waveform in [24] is designed by minimizing the interference at the communication user, but not SINR, which dictates the communication performance. The sensing signal in [23] cannot realize the maximum possible value of its degree of freedom when the number of users is smaller than the number of antennas [9]. The solutions proposed in [9], [23]–[25], [28]–[30] compute the rank-1 approximation of a full-rank Hermitian matrix to evaluate the ISAC waveform, which leads to degradation in performance. Moreover, the optimization criteria used in [9], [30] to compute the dedicated sensing signal do not include the communication signal, which effectively neglects the impact of the communication signal on sensing performance. In this paper, we optimize both the transmit communication precoding and dedicated sensing signal that form the ISAC waveform similar to [9], [25], [28]–[30]. The jointly optimized dedicated communication and sensing waveforms allow the sensing waveform to attain the maximum degree of freedom, equal to the number of antennas [9], [29]. We consider power-efficient communication aided by RIS to design individual communication signal, like [30].

This paper focuses on power-efficient, RIS-assisted waveform design using null-space projection and tunable sensing power. The RIS provides passive beamforming gain to achieve the required level of communication performance for each user with lower communication power compared to the case with no RIS, thus minimizing the effect of communication on sensing. In the absence of a direct channel between the BS and the communication user, the power needed to maintain a particular communication SINR level is still high. The sensing signal in [30] is designed without considering the precoded communication signal. However, the echo of the ISAC signal reflected off the target also consists of the reflected communication signal, which can interfere with the sensing signal and negatively impact sensing performance. As opposed to the route taken in [30], we include the communication signal in the design of the sensing signal as we aim to match the beampattern of the ISAC signal, not only the dedicated sensing signal, with the desired beampattern. This approach ensures that the communication signal power has a limited effect on sensing performance. Moreover, the ISAC signal in [30] utilizes the whole of the available transmit power. In contrast, the power of the sensing signal can be adjusted according to the required sensing SINR in our design, making it more efficient in terms of power utilization. The sensing signal is projected onto the null space of the communication channel to cancel its effect on the communication performance. This approach allows us to separate the problem of designing an ISAC waveform into two subproblems, *a* designing the communication precoder along with passive beamforming, and *b* the sensing signal. Our contributions can be summarized as follows.

(i) To determine the communication signal, we propose an alternating optimization-based solution that jointly optimizes the transmit precoder and the passive beamforming at the RIS to minimize communication power while guaranteeing a required communication SINR for each user.

(ii) We also propose a low-complexity, two-stage solution to determine the communication signal by minimizing the weighted sum of channel gains to compute passive beamforming, while minimizing the sum of lower limits of power to the individual users to evaluate transmit precoding.

(iii) We design the sensing signal by matching the beampattern of the ISAC signal with the desired beampattern, which is subsequently projected onto the null space of the communication channel. The power of the sensing signal is adjusted to fulfill the required sensing SINR at the receiver, which helps efficiently utilize the transmit power available. The proposed low complexity algorithm avoids the need to compute rank-1 approximation from the sensing covariance matrix, unlike [9], [23]–[25], [28]–[30].

The paper's novelty lies in designing the sensing signal with adjustable power to achieve the sensing SINR target, while integrating the communication signal into the sensing design to match the ISAC beampattern. This approach ensures that the communication signal's power minimally impacts sensing performance and the power is used efficiently.

A. Notations

$\mathbf{x}$ represents a vector, whereas $\mathbf{X}$ represents a matrix; x_i represents the i^{th} element of $\mathbf{x}$; $x_{i,j}$ represents the $(i,j)^{th}$ element of $\mathbf{X}$; $\mathbf{x}_k$ is the k^{th} column of $\mathbf{X}$; $\|\mathbf{x}\|$ is the $\ell 2$-norm of $\mathbf{x}$; $\|\mathbf{X}\|_F$ is the Frobenius norm of $\mathbf{X}$; $\mathrm{Tr}\left[\mathbf{X}\right]$ is the trace of $\mathbf{X}$; $\exp\left(\mathbf{X}\right)$ is a matrix whose $(i,j)^{th}$ entry is $\exp\left(x_{i,j}\right)$, where $\exp\left(.\right)$ is the exponential operator; $\mathbf{X}^{-1}$, $\mathbf{X}^{\dagger}$ and $\mathbf{X}^{H}$ are the inverse, pseudoinverse and Hermitian transpose of $\mathbf{X}$ respectively; $\odot$ is the Hadamard product of two matrices; $\mathrm{diag}\left(\mathbf{X}\right)$ is a column vector containing the diagonal elements of $\mathbf{X}$; $\mathrm{DIAG}\left(a_1,\ldots,a_n\right)$ is an $n\times n$ diagonal matrix with $a_1,\ldots,a_n$ as the diagonal elements; $\mathrm{DIAG}\left(\mathbf{x}\right)$ is a diagonal matrix with the elements of vector $\mathbf{x}$ as its diagonal elements; $\mathrm{BLKDIAG}(\mathbf{A}_1,\mathbf{A}_2,\ldots,\mathbf{A}_n)$ is a block-diagonal matrix in which $\mathbf{A}_1,\mathbf{A}_2,\ldots,\mathbf{A}_n$ form the diagonal; $\mathrm{rank}\left(\mathbf{X}\right)$ is the rank of $\mathbf{X}$; $\mathbf{I}_N$ is an $N\times N$ identity matrix; $\mathbb{R}_+$ denotes the set of positive real numbers; $\Re\left(\cdot\right)$ represents the real part of the argument; $\mathbb{E}[.]$ is the expectation operator; $\sim$ means 'has the probability distribution of'; $\triangleq$ means 'is defined as'; $\mathcal{N}(\mu,\sigma^2)$ represents complex Gaussian variable with mean μ and variance σ^2; $\mathcal{CN}(\boldsymbol{\mu},\mathbf{C})$ represents complex Gaussian vector with mean $\boldsymbol{\mu}$ and covariance matrix $\mathbf{C}$.

II. System Model

We consider an RIS-assisted ISAC system as shown in Fig. 1. The base station (BS), which serves the dual functions of communication and sensing, is equipped with N_t transmit antennas and N_r receive antennas to transmit the ISAC signal and receive its echoes for sensing, respectively. The BS serves K single-antenna communication user equipment (UEs) and sends radar probing signals to Q targets. We assume that $N_r \geq N_t \geq K$, which guarantees feasible precoding design and avoids the loss of information from sensed targets [8]. We consider an RIS having M elements deployed near the communication users to enhance communication.

Let $\mathbf{x}\in\mathbb{C}^{N_t\times 1}$ be the narrowband transmit downlink ISAC signal so that the received signal at K communication users is

$$\mathbf{y}_c = \mathbf{H}\mathbf{x} + \mathbf{n}_c, \tag{1}$$

where $\mathbf{H} = \left[\mathbf{h}_1^T,\mathbf{h}_2^T,\ldots,\mathbf{h}_K^T\right]^T$ is the communication channel from the BS to the users and $\mathbf{n}_c\in\mathbb{C}^{K\times 1}$ is the additive white Gaussian noise (AWGN) such that $\mathbf{n}_c\sim\mathcal{CN}\left(\mathbf{0},\sigma_c^2\mathbf{I}_K\right)$. The channel $\mathbf{h}_k$ from BS to the k^{th} user is devoid of the direct channel and composed of the composite BS-RIS-user channel,

$$\mathbf{h}_k = \mathbf{h}_{R,k}\boldsymbol{\Phi}\mathbf{H}_{BR}, \quad \forall\ k=1,2,\ldots,K, \tag{2}$$

where $\mathbf{h}_{R,k}\in\mathbb{C}^{1\times M}$ is the channel from the RIS to the k^{th} user, $\boldsymbol{\Phi}=\mathrm{diag}\left(\phi_1,\phi_2,\ldots,\phi_M\right)$ and $\mathbf{H}_{BR}\in\mathbb{C}^{M\times N_t}$ is the channel from the BS to the RIS. The transmit signal $\mathbf{x}$ is composed of a precoded communication signal and a dedicated radar probing signal as

$$\mathbf{x} = \mathbf{F}\mathbf{s}_c + \mathbf{s}_r, \tag{3}$$

where $\mathbf{F}\in\mathbb{C}^{N_t\times K}$ is the communication precoding matrix, $\mathbf{s}_c\in\mathbb{C}^{K\times 1}$ are the communication data streams and $\mathbf{s}_r\in\mathbb{C}^{N_t\times 1}$ is the dedicated sensing probing signal respectively. Even though the same ISAC signal $\mathbf{x}$ is used for both communication and sensing, we will refer to $\mathbf{F}\mathbf{s}_c$ as the communication signal and $\mathbf{s}_r$ as the sensing signal throughout the paper. The sample covariance matrix of the ISAC waveform $\mathbf{x}$ is

$$\mathbf{R}_x = (\mathbf{F}\mathbf{s}_c+\mathbf{s}_r)(\mathbf{F}\mathbf{s}_c+\mathbf{s}_r)^H = \mathbf{F}\mathbf{F}^H + \mathbf{R}_r, \tag{4}$$

where $\mathbf{R}_r\triangleq\mathbf{s}_r\mathbf{s}_r^H$. We make assumptions that the communication and sensing signals are statistically uncorrelated, *i.e.*, $\mathbb{E}\left[\mathbf{s}_c\mathbf{s}_r^H\right]=\mathbf{0}$ and $\mathbb{E}\left[\mathbf{s}_r\mathbf{s}_c^H\right]=\mathbf{0}$, the sample covariance matrices of communication and sensing probing signals are equal to their statistical counterparts, and $\mathbb{E}\left[\mathbf{s}_c\mathbf{s}_c^H\right]=\mathbf{I}$. We assume that the user channels are uncorrelated. Since we aim to minimize communication power with the aid of an RIS which eases the burden on precoder $\mathbf{F}$, we assume $\left\|\mathbf{F}\mathbf{s}_c\right\|^2 \ll \left\|\mathbf{s}_r\right\|^2$, and hence $\left\|\mathbf{x}\right\|^2\approx\left\|\mathbf{s}_r\right\|^2$ and $\left|x_m\right|^2\approx\frac{\left\|\mathbf{s}_r\right\|^2}{N_t}=\left|s_{r_m}\right|$. That is, most of the transmitted signal power is contributed by the sensing signal. However, this assumption might not hold true when dealing with moderate sensing SINR targets, correlated user channels, or imperfect RIS control. The echo signal reflected from the q^{th} sensing target at the receiver of BS is

$$\mathbf{y}_{r_q} = \sqrt{\tau_q}\mathbf{b}\left(\theta_q\right)\mathbf{a}\left(\theta_q\right)^H\mathbf{x} + \mathbf{n}_r,\ \forall q=1,2,\ldots,Q \tag{5}$$

where θ_q is the location of the q^{th} target in terms of azimuth angle relative to the BS, τ_q is the radar cross section of the q^{th} target, and $\mathbf{n}_r\in\mathbb{C}^{N_r\times 1}$ is the additive white Gaussian noise, *i.e.*, $\mathbf{n}_r\sim\mathcal{CN}\left(\mathbf{0},\sigma_r^2\mathbf{I}_{N_r}\right)$. $\mathbf{b}\left(\theta\right)\in\mathbb{C}^{N_r\times 1}$ and $\mathbf{a}\left(\theta\right)\in\mathbb{C}^{N_t\times 1}$ are the receive and the transmit steering vectors respectively. The reflection coefficient of the q^{th} target, $\alpha_q\propto\sqrt{\tau_q}$.

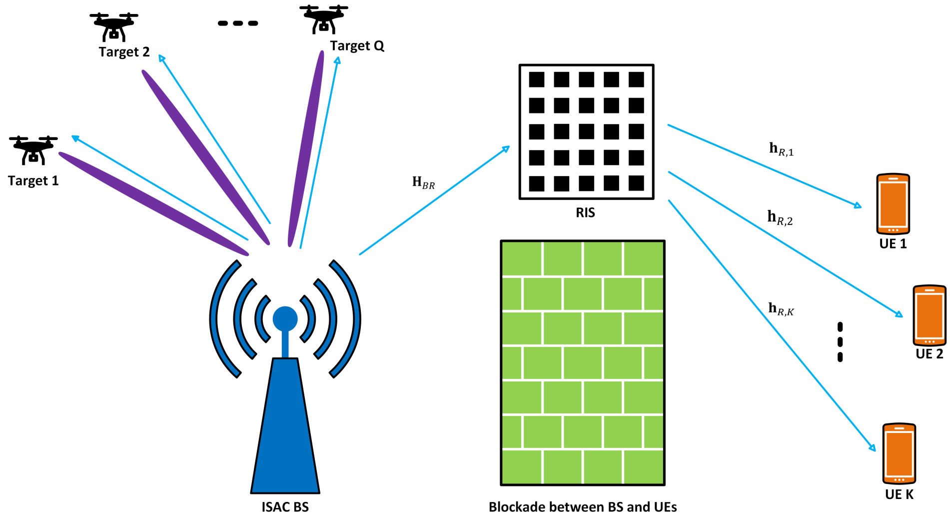

Fig. 1: RIS-aided integrated sensing and communication (ISAC)

The signal-to-interference-plus-noise ratio (SINR) at the k^{th} communication receiver is given by

$$\mathrm{SINR}_k = \frac{|\mathbf{h}_k \mathbf{f}_k|^2}{\sum_{\substack{i=1 \\ i \neq k}}^{K} |\mathbf{h}_k \mathbf{f}_i|^2 + |\mathbf{h}_k \mathbf{s}_r|^2 + \sigma_c^2} \quad \forall k = 1, 2, \ldots, K. \quad (6)$$

The power of the sensing probing signal is $P_r = \|\mathbf{s}_r\|^2$, and the power of the communication signal is given by

$$P_c = \mathbb{E}\left[\mathrm{Tr}\left(\mathbf{F}\mathbf{s}_c\mathbf{s}_c^H\mathbf{F}^H\right)\right] = \mathrm{Tr}\left[\mathbf{F}\mathbf{F}^H\right], \quad (7)$$

thus making the total transmit power $P_x = \|\mathbf{x}\|^2 = P_c + P_r$.

III. Problem Formulation

Our goal is to utilize transmit power to enhance ISAC performance efficiently. We seek to minimize both the transmit power of the communication signal and the difference between the ideal and actual beampattern of the ISAC signal. While we attempt to minimize transmit communication power, the minimum SINR must be maintained at each UE to ensure acceptable spectral efficiency, and the total transmit power cannot exceed a certain power level P_T, known as the maximum total transmit power. Since the communication power is minimized, most of the transmit power is available for the sensing signal, which allows us to maintain the required sensing SINR at the receiver. However, we can save additional transmit power by tuning the power of the dedicated sensing signal to meet only the required sensing SINR at the receiver.

A. Sensing performance

The dedicated sensing probe signal $\mathbf{s}_r$ is determined by minimizing the difference between the ideal and the actual beampatterns of the ISAC signal. The beampattern in the far-field at $\theta \in [-90^\circ,\ 90^\circ]$ is given by

$$B(\theta) = \left|\mathbf{a}(\theta)^H \mathbf{x}\right|^2. \quad (8)$$

The objective function for the beampattern design problem can be formulated as [34], [35]

$$\min_{\mathbf{x}} \quad \sum_{n=1}^{N} \left[d_n - \left|\mathbf{a}(\theta_n)^H \mathbf{x}\right|\right]^2, \quad (9)$$

where $\{\theta_n\}_{n=1}^N$ are the discrete angles obtained by dividing the interval $[-90^\circ,\ 90^\circ]$ into N sub-intervals and d_n is the desired beampattern at $\theta = \theta_n$. To counter the intractability of the objective function in (9) because of the $|.|$ operator, the authors in [34] introduce phase variable ϕ_n to make the problem tractable. The optimization problem (9) is reformulated as an optimization problem over ω_n and $\mathbf{s}_r$ as

$$\min_{\mathbf{x},\omega_n} \quad \sum_{n=1}^{N} \left|d_n e^{j\omega_n} - \mathbf{a}(\theta_n)^H \mathbf{x}\right|^2. \quad (10)$$

It is preferable for the waveform transmitted from each antenna for target probing to have a constant modulus, $i.e.|x_m|^2 = \frac{\|\mathbf{x}\|^2}{N_t}$. The optimization problem for determining the sensing signal can be written as

$$\min_{\mathbf{x}} \quad \|\mathbf{d} - \mathbf{A}\mathbf{x}\|^2 \quad (11a)$$

$$s.t. \quad |s_{r_m}| = \sqrt{\frac{P_T - P_c}{N_t}}, \quad m = 1, 2, \cdots, N_t, \quad (11b)$$

where

$$\mathbf{d} = \begin{bmatrix} d_1 \\ d_2 \\ \vdots \\ d_N \end{bmatrix} \text{ and } \mathbf{A} = \begin{bmatrix} \mathbf{a}(\theta_1)^H \\ \mathbf{a}(\theta_2)^H \\ \vdots \\ \mathbf{a}(\theta_N)^H \end{bmatrix}.$$

$\mathbf{s}_r$ is constrained to have constant modulus. For the time being, we consider $\mathbf{s}_r$ uses all the available power for sensing, *i.e.*, $P_r = P_T - P_c$, where P_T is the total power constraint. If the reflection coefficients or RCS of the sensing targets are known, we can adjust P_r by making sure the sensing SINR of each target at the receiver meets the minimum required sensing SINR, as shown in Section VI-C.

B. Communication performance

For each user k the numerator of the SINR, $|\mathbf{h}_k\mathbf{f}_k|^2 \ll |\mathbf{h}_k\mathbf{s}_r|^2$. We ensure $|\mathbf{h}_k\mathbf{s}_r|^2 = 0$ by making sure $\mathbf{s}_r$ lies in the null space of channel $\mathbf{H}$, which helps in achieving the same SINR with much smaller communication power. As a result, the SINR for the k^{th} user reduces to

$$\text{SINR}_k = \frac{|\mathbf{h}_k\mathbf{f}_k|^2}{\sum\limits_{\substack{i=1\\i\neq k}}^{K} |\mathbf{h}_k\mathbf{f}_i|^2 + \sigma_c^2} \;\; \forall k = 1, 2, \ldots, K. \quad (12)$$

The optimization problem of minimizing communication power can be described as

$$\min_{\mathbf{F}} \quad \text{Tr}\left[\mathbf{F}\mathbf{F}^H\right] \quad (13a)$$

$$s.t. \frac{|\mathbf{h}_k\mathbf{f}_k|^2}{\sum\limits_{i=1, i\neq k}^{K} |\mathbf{h}_k\mathbf{f}_i|^2 + \sigma_c^2} \geq \gamma_k, \; \forall k = 1, \ldots, K \quad (13b)$$

where γ_k is the minimum SINR requirement for the user k. Without loss of generality, it is assumed that the communication power $\text{Tr}\left[\mathbf{F}\mathbf{F}^H\right]$ required to achieve the given SINR is much smaller than P_T, the maximum total transmit power.

We observe that the communication performance is not dependent on the sensing signal; however, the sensing performance is dependent on the communication signal. Thus, we determine the communication signal first, which depends on the computation of transmit precoding $\mathbf{F}$ and passive beamforming $\mathbf{\Phi}$ at the RIS. After determining the communication signal, we optimize sensing performance to compute the sensing signal, keeping the communication signal constant.

IV. Alternating Optimization Based Solution for Communication Signal

A. Minimum power precoding solution

The problem (13) can be translated into a second-order cone programming (SOCP) [36] as

$$\min_{\mathbf{F}} \quad \kappa \quad (14a)$$

$$s.t. \sqrt{1 + \frac{1}{\gamma_k}}\mathbf{h}_k\mathbf{f}_k \geq \left\| \begin{bmatrix} \mathbf{h}_k\mathbf{F} \\ \sigma_c \end{bmatrix} \right\|, \; \forall k = 1, \ldots, K, \quad (14b)$$

$$\sum_{k=1}^{K} \|\mathbf{f}_k\| \leq \kappa, \quad (14c)$$

which can be easily solved using cvx [37]. The channel $\mathbf{H}$, however, is dependent on $\mathbf{\Phi}$, which is unknown to solve problem (14). Thus, we can initialize $\mathbf{\Phi}$ with a random but valid value and solve (14) for $\mathbf{F}$. In the next step, we solve for $\mathbf{\Phi}$ using the obtained value of $\mathbf{F}$. We solve for $\mathbf{F}$ and $\mathbf{\Phi}$ alternately until convergence.

B. Passive Beamforming Solution

The objective value in (14a) is not dependent on $\mathbf{\Phi}$, and only the constraint (14b) is dependent on $\mathbf{\Phi}$. We may choose any $\mathbf{\Phi}$ that satisfies constraint (14b), which would reduce it to the *feasibility-check* problem.

However, we seize this opportunity to leverage the passive beamforming furnished by the RIS to enhance the communication performance. We define an objective function that seeks to maximize the minimum SINR for all users and optimize the passive beamforming or the RIS phase-shift matrix $\mathbf{\Phi}$,

$$\max_{\mathbf{\Phi}} \quad \nu \quad (15a)$$

$$s.t. \quad \frac{\text{Tr}[\bar{\mathbf{H}}_k^H \mathbf{R}_\phi \bar{\mathbf{H}}_k \mathbf{R}_{F,k}]}{\sum\limits_{i=1, i\neq k}^{K} \text{Tr}[\bar{\mathbf{H}}_k^H \mathbf{R}_\phi \bar{\mathbf{H}}_k \mathbf{R}_{F,i}] + \sigma_c^2} \geq \nu, \; \forall k = 1, \ldots, K, \quad (15b)$$

$$\text{diag}\left(\mathbf{R}_\phi\right) = \mathbf{1}, \quad (15c)$$

$$\mathbf{R}_\phi \succeq \mathbf{0}, \quad (15d)$$

$$\text{rank}\left(\mathbf{R}_\phi\right) = 1, \quad (15e)$$

where $\bar{\mathbf{H}}_k \triangleq \text{diag}(\mathbf{h}_{R,k})\mathbf{H}_{BR}$, $\mathbf{R}_{F,k} \triangleq \mathbf{f}_k\mathbf{f}_k^H$ and $\mathbf{R}_\phi \triangleq \boldsymbol{\phi}\boldsymbol{\phi}^H$. The term on the left-hand side of (15b) represents the SINR for the k^{th} user. We relax the non-convex rank-1 constraint and reformulate the problem as a semidefinite programming problem (SDP),

$$\max_{\boldsymbol{\phi}} \quad \nu \quad (16a)$$

$$s.t. \quad \text{Tr}[\bar{\mathbf{H}}_k^H \mathbf{R}_\phi \bar{\mathbf{H}}_k \mathbf{R}_{F,k}] \geq \nu \left[\sum_{i=1, i\neq k}^{K} \text{Tr}[\bar{\mathbf{H}}_k^H \mathbf{R}_\phi \bar{\mathbf{H}}_k \mathbf{R}_{F,i}] + \sigma_c^2 \right], \; \forall k = 1, \ldots, K, \quad (16b)$$

$$\text{diag}\left(\mathbf{R}_\phi\right) = \mathbf{1}, \quad (16c)$$

$$\mathbf{R}_\phi \succeq \mathbf{0}, \quad (16d)$$

By relaxing the rank-1 constraint on $\mathbf{R}_\phi$, we make the optimization problem convex. If the solution to the SDP has rank one, the relaxation is tight, and the solution is also optimal for the original problem. However, when the SDP returns a solution of rank greater than one, we need to approximate a rank-1 solution from the SDP solution, thus making the relaxation-based solution suboptimal. The optimization problem (16) is quasi-convex because for any value of ν, the feasible set in (16) is convex. We can combine the bisection search algorithm with the feasibility-check problem to solve the problem (16). We determine the maximum feasible value of ν within an interval by using the bisection search algorithm.

Algorithm 1 Alternating Optimization Based Algorithm

Require: $\mathbf{h}_{R,k}, \mathbf{H}_{BR}, \gamma_k, \sigma_c$.

1: Initialize $\mathbf{\Phi}^{(0)} = \mathrm{diag}\left(\exp\left(j\boldsymbol{\psi}\right)\right)$, where $\boldsymbol{\psi}$ is N_t-length column vector and $\boldsymbol{\psi}_i,\ i = 1, \dots, N_t$ are random phase angles, and set $k = 1$.
2: **repeat**
3: Solve problem (14) for $\mathbf{F}$ using cvx.
4: Compute $\bar{\mathbf{H}}_k = \mathrm{diag}(\mathbf{h}_{R,k})\mathbf{H}_{BR}$, $\mathbf{R}_{F,k} = \mathbf{f}_k\mathbf{f}_k^H\ \ \forall k = 1, 2, \dots, K$.
5: Solve problem (16) for $\mathbf{R}_\phi = \boldsymbol{\phi}\boldsymbol{\phi}^H$. Compute $\boldsymbol{\phi}$ from $\mathbf{R}_\phi$.
6: $k \leftarrow k + 1$.
7: **until** convergence, *i.e.*, $\left\|\mathbf{F}^{(k)}\right\|_F^2 - \left\|\mathbf{F}^{(k-1)}\right\|_F^2 \leq \epsilon_{tol}$, a small positive value or $k \geq iter_{max}$, where $iter_{max}$ is the maximum of number of iterations.
8: Compute $\mathbf{s}_r$ by solving problem (11) using Algorithm
9: **return** $\mathbf{F}, \mathbf{\Phi}$ and $\mathbf{s}_r$.

The feasibility problem to determine the feasibility of a value of ν can be written as

$$\begin{aligned} &\text{Find} \quad \boldsymbol{\phi} \\ &s.t. \quad \text{(16b), (16c), (16d).} \end{aligned} \tag{17}$$

The feasibility problem (17) with SINR constraints to determine $\boldsymbol{\phi}$ is first solved for $\mathbf{R}_\phi$ which is a semidefinite programming (SDP) problem that can be solved using cvx, following the procedure summarized in Algorithm 2. We can approximate $\boldsymbol{\phi}$ from the obtained $\mathbf{R}_\phi$ either using a Gaussian randomization or the dominant singular value decomposition (SVD) vector. In this paper, we obtain the dominant SVD vector of $\mathbf{R}_\phi$ and normalize its each element to unit amplitude so that the diagonal constraint is satisfied to recover $\boldsymbol{\phi}$ from $\mathbf{R}_\phi$.

Algorithm 2 Passive Beamforming Algorithm

Require: $\bar{\mathbf{H}}_k$, $\mathbf{R}_{F,k}$, σ_c, γ_k, ν_{max}.

1: Set $\nu_{min} = \min\left(\gamma_k\right)$.
2: **repeat**
3: $\nu = \left(\nu_{min} + \nu_{max}\right)/2$
4: Solve problem (17). If the problem is feasible for ν, set $\nu_{min} = \nu$ and $\mathbf{R}_\phi^{sol} = \mathbf{R}_\phi$ where $\mathbf{R}_\phi$ is the solution of (17). Otherwise, set $\nu_{max} = \nu$.
5: **until** convergence, *i.e.*, $\nu_{max} - \nu_{min} \leq \epsilon_{tol}$, a convergence threshold.
6: **return** $\mathbf{R}_\phi^{sol}$ as solution.

V. Two-stage low complexity solution for Communication signal

The solution based on alternating optimization in Section IV is cumbersome and computationally complex because of both the alternating optimization and multiple executions of the feasibility-check algorithm, especially for the system with large arrays of transmit antennas and/or RIS. In this section, we propose a low complexity algorithm where we first fix RIS phase-shifts and then determine the minimum power precoding solution.

A. Manifold optimization-based passive beamforming solution

We use the asymptotic beamforming property to develop an optimization problem for RIS phase-shifts. Zero-forcing (ZF) precoder is asymptotically optimal at high signal-to-noise ratio (SNR) regime where the system is interference-limited [38]–[40]. Considering the ZF precoder at the transmitter, we aim to frame an optimization problem for RIS phase-shifts. The ZF precoder is computed as

$$\mathbf{F}_{ZF} = \left(\mathbf{H}\mathbf{H}^H\right)^{-1}\mathbf{H}^H\mathbf{P}_{ZF}^{\frac{1}{2}} = \mathbf{H}^\dagger\mathbf{P}_{ZF}^{\frac{1}{2}}, \tag{18}$$

where $\mathbf{P}_{ZF}$ is the power allocation matrix, and $\mathbf{P}_{ZF} = \mathrm{diag}\left(\gamma_1\sigma_c^2, \gamma_2\sigma_c^2, \dots, \gamma_K\sigma_c^2\right)$ to satisfy individual SINR constraints. Since we are trying to minimize power, the objective function for determining RIS phase-shifts $\boldsymbol{\phi} = \mathrm{diag}\left(\mathbf{\Phi}\right)$ is

$$\min_{\boldsymbol{\phi}} \quad \mathrm{Tr}\left[\mathbf{F}_{ZF}\mathbf{F}_{ZF}^H\right] = \mathrm{Tr}\left[\left(\mathbf{H}^H\mathbf{P}_{ZF}^{-1}\mathbf{H}\right)^\dagger\right] \tag{19}$$

Using the results from Appendix A, we can write

$$\mathrm{Tr}\left[\left(\mathbf{H}^H\mathbf{P}_{ZF}^{-1}\mathbf{H}\right)^\dagger\right] \geq \frac{r^2}{\mathrm{Tr}\left[\left(\mathbf{H}^H\mathbf{P}_{ZF}^{-1}\mathbf{H}\right)\right]}, \tag{20}$$

where $r = \mathrm{rank}\left(\mathbf{H}^H\mathbf{P}_{ZF}^{-1}\mathbf{H}\right)$. In order to develop a low complexity solution, we choose to minimize the lower limit of the objective function in (20), similar to the approach taken in [41],

$$\max_{\boldsymbol{\phi}} \quad \mathrm{Tr}\left[\mathbf{H}^H\mathbf{P}_{ZF}^{-1}\mathbf{H}\right] \tag{21a}$$

$$s.t. \qquad |\boldsymbol{\phi}_m| = 1, \quad m = 1, 2, \dots, m. \tag{21b}$$

The objective function (21a) can be expressed as

$$\begin{aligned} &\mathrm{Tr}\left[\mathbf{H}^H\mathbf{P}_{ZF}^{-1}\mathbf{H}\right] \\ =&\sum_{k=1}^{K}\frac{1}{\gamma_k\sigma_c^2}\mathbf{v}^H\left(\mathbf{H}_{r,k}\mathbf{H}_{BR}\mathbf{H}_{BR}^H\mathbf{H}_{r,k}^H\right)\mathbf{v} \\ =&\sum_{k=1}^{K}\mathbf{v}^H\mathbf{R}_{H_k}\mathbf{v} \\ =&\mathbf{v}^H\left(\sum_{k=1}^{K}\mathbf{R}_{H_k}\right)\mathbf{v} \end{aligned}$$

where $\mathbf{v} \triangleq \boldsymbol{\phi}^*$, $\mathbf{R}_{H_k} \triangleq \frac{1}{\gamma_k\sigma_c^2}\left(\mathbf{H}_{r,k}\mathbf{H}_{BR}\mathbf{H}_{BR}^H\mathbf{H}_{r,k}^H\right)$ and $\mathbf{H}_{r,k} = \mathrm{diag}\left(\mathbf{h}_{r,k}\right)\mathbf{H}_{BR}$. We rewrite the optimization problem (21) in terms of the optimization problem for $\mathbf{v}$,

$$\max_{\mathbf{v}} \quad \mathbf{v}^H\mathbf{R}_H\mathbf{v} \tag{22a}$$

$$s.t. \qquad |v_m| = 1, \quad m = 1, 2, \dots, M, \tag{22b}$$

where $\mathbf{R}_H \triangleq \sum_{k=1}^K \mathbf{R}_{H_k} \in \mathbb{C}^{M\times M}$ is a Hermitian semidefinite matrix. The optimization problem in (22) is a nonconvex, NP-hard problem [35], [42]. We adopt a manifold optimization approach to solve problem (22), as $\mathbf{v}$ represents a complex circle manifold. We start with a light introduction to manifolds.

Algorithm 3 Armijo Backtracking Line Search

Require: Function $f(\mathbf{X})$, gradient ∇f, current point $\mathbf{X}$, descent direction z, initial step size $\alpha_0 > 0$, reduction factor $\rho \in (0,1)$, Armijo constant $c \in (0,1)$
Ensure: Step size α satisfying the Armijo condition
1: Initialize $\alpha \leftarrow \alpha_0$
2: Compute $f_{\mathbf{X}} \leftarrow f(\mathbf{X})$
3: Compute $\nabla f_{\mathbf{X}} \leftarrow \nabla f(\mathbf{X})$
4: **while** $f(\mathbf{X} + \alpha z) > f_{\mathbf{X}} + c\alpha \nabla f_{\mathbf{X}}^T z$ **do**
5: $\quad \alpha \leftarrow \rho\alpha$
6: **end while**
7: **return** α

a) Introduction to Manifolds: Manifold is a topological space that looks like an Euclidean space locally [43]. Riemannian manifold, in particular, has the inner product defined on each tangent space, known as Riemannian metric. Tangent space at a point x on the manifold $\mathcal{M}$, denoted by $T_x\mathcal{M}$, is the vector space that consists of all tangent vectors to the curves on the manifold passing through the point x [44]. Riemannian metric allows us to define geometric concepts such as lengths, angles, and distances on the manifolds [43]. Riemannian manifold enables the use of calculus and defining of gradients so that optimization can be performed [44].

The feasible set of problem in (22) can be viewed as a product of M complex unit circles where each complex circle $\mathcal{S}$ is defined as $\mathcal{S} \triangleq \{x \in \mathbb{C} : |x| = xx^* = 1\}$. The product of M such unit circles is called the complex circle manifold which is defined as

$$\mathcal{M}_{cc}^M = \left\{\mathbf{x} \in \mathbb{C}^M : |x_m| = x_m x_m^* = 1, m = 1, 2, \ldots, M\right\} \tag{23}$$

Tangent space at point $\mathbf{x} \in \mathcal{M}_{cc}^M$ is defined as

$$T_{\mathbf{x}}\mathcal{M}_{cc}^M = \left\{\mathbf{y} \in \mathbb{C}^M : \Re\left(\mathbf{x}^* \odot \mathbf{y}\right) = \mathbf{0}_M\right\} \tag{24}$$

The complex circle manifold $\mathcal{M}_{cc}^M$ is a Riemannian submanifold of $\mathbb{C}^M$.

b) Optimization over manifolds: We briefly explain how optimization is performed over manifold. Consider the optimization of a smooth real-valued function $\mathbf{x}$ over a manifold $\mathcal{M}^M$,

$$\min_{\mathbf{x} \in \mathcal{M}^M} \quad f(\mathbf{x}) \tag{25}$$

The modified form of line search based algorithms used in Euclidean space are employed in optimization over manifolds [35]. Riemannian gradient represents the direction of steepest ascent for a function $f(\mathbf{x})$ on manifold, and hence the negative of Riemannian gradient is used as the direction of descent while minimizing the function on a manifold. In general, we repeat following steps until convergence during optimization over manifolds.

- The Riemannian gradient of a function $f(\mathbf{x})$ at point $\mathbf{x}^{(k)}$ is computed by projecting the Euclidean gradient $\nabla f(\mathbf{x})$ onto the tangent space $T_{\mathbf{x}^{(\mathbf{k})}}\mathcal{M}^M$ by means of a projection operator [45],

$$\begin{aligned} \mathrm{grad}_{\mathbf{x}^{(k)}} f(\mathbf{x}) &= \mathrm{Proj}_{\mathbf{x}^{(k)}} \nabla f(\mathbf{x}) \\ &= \nabla f(\mathbf{x}) - \Re\left\{\nabla f(\mathbf{x}) \odot \mathbf{x}^*\right\} \odot \mathbf{x} \end{aligned} \tag{26}$$

- The update is performed on the tangent space along the direction of the projection at $\mathbf{x}^{(k)}$ which is $\mathrm{Proj}_{\mathbf{x}} \nabla f\left(\mathbf{x}^{(k)}\right)$,

$$\bar{\mathbf{x}}^{(k)} = \mathbf{x}^{(k)} - \beta^{(k)} \,\mathrm{Proj}_{\mathbf{x}^{(k)}} \nabla f\left(\mathbf{x}^{(k)}\right),\ \bar{\mathbf{x}}^{(k)} \in T_{\mathbf{x}^{(k)}}\mathcal{M}^M, \tag{27}$$

  where $\beta^{(k)}$ is the step-size that ensures that the objective function is non-increasing at each iteration. Armijo backtracking line search step is used to guarantee the objective function to be non-increasing in each iteration.
- Finally, $\bar{\mathbf{x}}^{(k)}$ needs to be mapped back to the manifold $\mathcal{M}^M$ using the retraction operator as,

$$\mathbf{x}^{(k+1)} = \mathrm{Retr}_{\mathbf{x}^{(k)}}\left(\bar{\mathbf{x}}^{(k)}\right), \tag{28}$$

  where $\mathrm{Retr}_{\mathbf{x}^{(k)}}(\cdot)$ is the retraction operator that maps a tangent vector at point $\mathbf{x}_k$ on manifold $\mathcal{M}^M$ to the manifold $\mathcal{M}^M$ itself.

For more details on optimization over manifolds, we suggest the readers to refer [43], [45], [46]. Next, we develop the manifold based optimization for solving (22). Following [35], we make a slight adjustment in the objective function in (22) and rewrite it as a minimization problem,

$$\min_{\mathbf{v}} \quad -\mathbf{v}^H\left(\mathbf{R}_H - \alpha\mathbf{I}\right)\mathbf{v} \tag{29a}$$

$$s.t. \quad |v_m| = 1, \quad m = 1, 2, \ldots, M, \tag{29b}$$

where $\alpha \geq 0$ is used to control convergence. It is shown in [35] that α should be chosen such that $\alpha \geq \frac{M}{8}\lambda_{R_H}$ to ensure convergence, where λ_{R_H} is the largest eigenvalue of $\mathbf{R}_H$. The addition of $\alpha\mathbf{v}^H\mathbf{v} = \alpha M$ to the objective function makes no difference to the optimization problem and its solution as αM is only a constant.

We summarize the procedure of solving the optimization problem (30) with the manifold based optimization technique in [35]. The Euclidean gradient of the cost function in (29a), $f(\mathbf{v}) = -\mathbf{v}^H\left(\mathbf{R}_H - \alpha\mathbf{I}\right)\mathbf{v}$ is

$$\nabla f(\mathbf{v}) = -2\left(\mathbf{R}_H - \alpha\mathbf{I}\right)\mathbf{v} \tag{30}$$

The problem is solved iteratively by performing following steps at each iteration k:

(i) The gradient $\nabla f(\mathbf{v})$ is projected onto the tangent space $T_{\mathbf{v}^{(k)}}\mathcal{M}_{cc}^M$ at point $\mathbf{v}^{(k)}$ on the complex circle manifold $\mathcal{M}_{cc}^M$ using the relation (26) which gives the Riemannian gradient.

(ii) The current value of $\mathbf{v}^{(k)}$ on the tangent space $T_{\mathbf{v}^{(k)}}\mathcal{M}_{cc}^{M}$ is updated to $\bar{\mathbf{v}}^{(k)}$ using the relation (27). In our Algorithm 4 to solve (23), we employ Manopt toolbox for MATLAB [47] which uses Armijo backtracking line search to guarantee that the objective function is non-increasing. Alternatively, the value of β can be chosen as $0 < \beta < \frac{1}{\lambda_{\mathbf{R}_H + \gamma \mathbf{I}}}$ where $\lambda_{\mathbf{R}_H + \gamma \mathbf{I}}$ is the largest eigenvalue of $\mathbf{R}_H + \gamma \mathbf{I}$, as suggested in [35]. Armijo backtracking line search uses a variable step size unlike [35].

(iii) The update on the tangent space is retracted back to manifold $\mathcal{M}_{cc}^{M}$ by using the retraction operator,

$$\mathrm{Retr}_{\mathbf{v}^{(k)}}\left(\bar{\mathbf{v}}^{(k)}\right) = \bar{\mathbf{v}}^{(k)} \odot \frac{1}{\left|\bar{\mathbf{v}}^{(k)}\right|}, \tag{31}$$

where $\left|\bar{\mathbf{v}}^{(k)}\right|$ represents a vector with entries equal to the absolute values of corresponding elements of $\bar{\mathbf{v}}^{(k)}$.

Algorithm 4 Steepest Descent Algorithm for Passive Beamforming Based on Manifold Optimization

Require: Cost function $f(\mathbf{v})$, initial $\mathbf{v}^{(0)}$ and convergence threshold ϵ_{tol}.
1: Set $k = 0$.
2: **repeat**
3: Evaluate Euclidean gradient of the cost function: $\nabla f\left(\mathbf{v}^{(k)}\right)$.
4: Evaluate the projection of $\nabla f\left(\mathbf{v}^{(k)}\right)$ onto the tangent space $T_{\mathbf{v}^{(k)}}\mathcal{M}_{cc}^{M}$ using (33).
5: Compute the step size β using Armijo Backtracking Line search method
6: Update the current value of $\mathbf{v}^{(k)}$ on the tangent space $T_{\mathbf{v}^{(k)}}\mathcal{M}_{cc}^{M}$ to $\bar{\mathbf{v}}^{(k)}$ using (34).
7: Evaluate the next iterate by retracting $\bar{\mathbf{v}}^{(k)}$ back to the complex circle manifold using the relation $\mathbf{v}^{(k+1)} = \mathrm{Retr}_{\mathbf{v}^{(k)}}\left(\bar{\mathbf{v}}^{(k)}\right)$, where $\mathrm{Retr}_{\mathbf{v}^{(k)}}\left(\bar{\mathbf{v}}^{(k)}\right)$ is computed using (38).
8: **until** convergence, *i.e.*, $\left|f\left(\mathbf{v}^{(k+1)}\right) - f\left(\mathbf{v}^{(k)}\right)\right| \le \epsilon_{tol}$.
9: **return** $\mathbf{v}^{(k+1)}$ as the solution.

B. Minimum power precoding for communication

We develop a low complexity algorithm to determine minimum power precoding solution to minimize communication power. We consider that the precoder $\mathbf{F} = \mathbf{U}\mathbf{P}^{\frac{1}{2}}$, where $\mathbf{U} \in \mathbb{C}^{N_t \times K}$ has unit norm columns and $\mathbf{P}$ is a diagonal matrix. $\mathbf{P} = \mathrm{DIAG}(\mathbf{p})$ where $\mathbf{p} \triangleq [p_1, p_2, \ldots, p_K]^T$ and $\{p_k\}_{k=1}^{K}$ represent the power intended for the k^{th} user. We can rewrite the optimization problem as,

$$\min_{\mathbf{U},\mathbf{P}} \quad \sum_{k=1}^{K} p_k \tag{32a}$$

$$s.t.\ p_k = \gamma_k \frac{\sum\limits_{i=1, i\neq k}^{K} |\mathbf{h}_k \mathbf{u}_i|^2 p_i + \sigma_c^2}{|\mathbf{h}_k \mathbf{u}_k|^2},\ \forall k = 1, \ldots, K \tag{32b}$$

$$\|\mathbf{u}_k\|^2 = 1,\ k = 1, \ldots, K, \tag{32c}$$

where we assume that the total power required to achieve the given SINR constraints is much smaller than the maximum transmit power allowed. The constraint (32b) is obtained by rearranging the constraint (13b). In (32b), we have only taken the lower limit of p_k as it gives the minimum p_k. We can see that the two optimization variables are coupled. Hence, we solve for one variable at one time while another is kept fixed. Assuming $\{p_k\}_{k=1}^{K}$ is known, we can rewrite optimization problem (32) as an optimization problem for $\mathbf{U}$,

$$\min_{\mathbf{U}} \quad \sum_{k=1}^{K} \gamma_k \frac{\sum\limits_{i=1, i\neq k}^{K} |\mathbf{h}_k \mathbf{u}_i|^2 p_i + \sigma_c^2}{|\mathbf{h}_k \mathbf{u}_k|^2} \tag{33a}$$

$$s.t. \quad |\mathbf{u}_k|^2 = 1,\ k = 1, \ldots, K, \tag{33b}$$

where we have replaced p_k in (32a) with the expression given by (32b). As $\mathbf{U}$ lies on the complex oblique manifold, we propose to solve the optimization problem (33) by using steepest descent algorithm on complex oblique manifold. Complex oblique manifold $\mathcal{M}_{OB}^{n\times m}$ is a Riemannian submanifold and defined as a set of complex matrices with unit-norm columns, *i.e.*,

$$\mathcal{M}_{OB}^{n\times m} = \left\{\mathbf{X} \in \mathbb{C}^{n\times m} : \|\mathbf{x}_j\| = 1\ \forall j = 1, 2, \ldots, m\right\} \tag{34}$$

Algorithm 5 Steepest Descent Algorithm for Precoding Based on Manifold Optimization

Require: Cost function $g(\mathbf{U})$, initial $\mathbf{U}^{(0)}$ and convergence threshold ϵ_{tol}.
1: Set $j = 0$.
2: **repeat**
3: Evaluate Euclidean gradient of the cost function: $\nabla g\left(\mathbf{U}^{(j)}\right)$.
4: Evaluate the projection of $\nabla g\left(\mathbf{U}^{(j)}\right)$ onto the tangent space $T_{\mathbf{U}^{(j)}}\mathcal{M}_{OB}^{N_t\times K}$ using (43).
5: Compute the step size $\beta^{(j)}$ using Armijo Backtracking Line search method
6: Update the current value of $\mathbf{U}^{(j)}$ on the tangent space $T_{\mathbf{U}^{(j)}}\mathcal{M}_{OB}^{N_t\times K}$ to $\bar{\mathbf{U}}^{(j)}$ using (37).
7: Evaluate the next iterate by retracting $\bar{\mathbf{U}}^{(j)}$ back to the complex oblique manifold using the relation $\mathbf{U}^{(j+1)} = \mathrm{Retr}_{\mathbf{U}^{(j)}}\left(\bar{\mathbf{U}}^{(j)}\right)$, where $\mathrm{Retr}_{\mathbf{U}^{(j)}}\left(\bar{\mathbf{U}}^{(j)}\right)$ is computed using (39).
8: **until** convergence, *i.e.*, $\left|g\left(\mathbf{U}^{(j+1)}\right) - g\left(\mathbf{U}^{(j)}\right)\right| \le \epsilon_{tol}$.
9: **return** $\mathbf{U}^{(j+1)}$ as the solution.

The problem (33) is solved iteratively by steepest descent algorithm on complex oblique manifold $\mathcal{M}_{OB}^{N_t\times K}$ by pursuing the following steps at each iteration j:

(i) The Euclidean gradient $\nabla g(\mathbf{U})$ where $g(\mathbf{U})$ is the

Algorithm 6 Iterative Algorithm to compute communication power allocation

---

Require: $\mathbf{H}$, σ_c, γ_k, convergence threshold ϵ_{tol}, $\mathbf{U}$ and the initial power allocation vector $\mathbf{p}^{(0)}$.

Set iteration index $j \leftarrow 1$.
repeat
  Set $\mathbf{p}^{(j)} = \mathbf{p}^{(j-1)}$
  for $k = 1, 2, \ldots, K$ **do**
    Update $p_k^{(j)} = \gamma_k \frac{\sum_{i=1, i\neq k}^{K} \|\mathbf{h}_k \mathbf{u}_i\|^2 p_i^{(j)} + \sigma_c^2}{\|\mathbf{h}_k \mathbf{u}_k\|^2}$
  end for
  $j \leftarrow j + 1$
until convergence, *i.e.*, $\left\|\mathbf{p}^{(j)} - \mathbf{p}^{(j-1)}\right\| \leq \epsilon_{tol}$.
return $\mathbf{p}^{(j)}$

---

objective function in (33a) is given by

$$\nabla g(\mathbf{U}) = -2\gamma_k \frac{\sum_{i=1, i\neq k}^{K} |\mathbf{h}_k \mathbf{u}_i|^2 p_i + \sigma_c^2}{|\mathbf{h}_k \mathbf{u}_k|^4} \mathbf{h}_k^H \mathbf{h}_k \mathbf{u}_k + \sum_{i=1, i\neq k}^{K} \frac{2\gamma_i \mathbf{h}_i^H \mathbf{h}_i \mathbf{u}_k p_k}{|\mathbf{h}_i \mathbf{u}_i|^2} \tag{35}$$

Riemannian gradient is evaluated at current iterate $\mathbf{U}^{(j)}$ by projecting the Euclidean gradient $\nabla g\left(\mathbf{U}^{(j)}\right)$ onto the tangent space at point $\mathbf{U}^{(j)}$ on the complex oblique manifold $\mathcal{M}_{OB}^{N_t \times K}$ using the relation,

$$\begin{aligned} &\text{grad } g\left(\mathbf{U}^{(j)}\right) \\ =&\,\text{Proj}\,\nabla g\left(\mathbf{U}^{(j)}\right) \\ =&\nabla g\left(\mathbf{U}^{(j)}\right) - \Re\left\{\text{DIAG}\left({\mathbf{U}^{(j)}}^H \nabla g\left(\mathbf{U}^{(j)}\right)\right)\right\} \odot \mathbf{U}^{(j)} \end{aligned} \tag{36}$$

(ii) The current value of $\mathbf{U}^{(j)}$ on the tangent space is updated to $\bar{\mathbf{U}}^{(j)}$ using the relation,

$$\bar{\mathbf{U}}^{(j)} = \mathbf{U}^{(j)} - \beta^{(j)}\,\text{Proj}\,\nabla g\left(\mathbf{U}^{(j)}\right), \tag{37}$$

where $\bar{\mathbf{U}}^{(j)} \in T_{\mathbf{U}^{(j)}} \mathcal{M}_{OB}^{N_t \times K}$, the tangent space at $\mathbf{U}^{(j)}$. Armijo backtracking line search is used to determine step size $\beta^{(j)}$.

(iii) The update on the tangent space is retracted back to manifold $\mathcal{M}_{OB}^{N_t \times K}$ by using the retraction operator,

$$\text{Retr}_{\mathbf{U}^{(j)}}\left(\bar{\mathbf{U}}^{(j)}\right) = \left[\frac{\bar{\mathbf{u}}_1^{(j)}}{\left\|\bar{\mathbf{u}}_1^{(j)}\right\|}, \ldots, \frac{\bar{\mathbf{u}}_K^{(j)}}{\left\|\bar{\mathbf{u}}_K^{(j)}\right\|}\right], \tag{38}$$

where we have normalized each column of $\bar{\mathbf{U}}^{(j)}$, the update on the tangent space. We have summarized the algorithm to compute $\mathbf{U}$ when $\mathbf{p}$ is known in Algorithm 5

Algorithm 7 Two Stage Algorithm based on Manifold Optimization

---

Require: $\mathbf{H}, \{\gamma_k\}_{k=1}^{K}, \sigma_c$ and convergence threshold ϵ_{tol}.

Initialize power for each user $\mathbf{p}^{(0)} = \left[\gamma_1 \sigma_c^2, \ldots, \gamma_K \sigma_c^2\right]$. Set iteration index $j \leftarrow 1$.
repeat
  Solve problem (33) for $\mathbf{U}^{(j)}$ using Algorithm 5 with $\mathbf{p}^{(j-1)}$ as power vector.
  Evaluate $\mathbf{p}^{(j)}$ using Algorithm 6 .
  $j \leftarrow j + 1$.
until convergence, *i.e.*, $\left|f\left(\mathbf{U}^{(j)}, \mathbf{p}^{(j)}\right) - f\left(\mathbf{U}^{(j-1)}, \mathbf{p}^{(j-1)}\right)\right|^2 \leq \epsilon_{tol}$ where $f(\mathbf{U}, \mathbf{p})$ is given by (33) and we take $\mathbf{U}^{(0)}$ as a matrix where column k has all zeros except 1 at the k^{th} position.
return $\mathbf{F} = \mathbf{U}^{(j)} \mathbf{P}^{(j)^{\frac{1}{2}}}$.

Finally, we can compute $\{p_k\}_{k=1}^{K}$ from (32b) if $\mathbf{U}$ is known. As p_k depends on the values of $\{p_i\}_{i=1, i\neq k}^{K}$, we can take initial value of $\{p_k\}_{k=1}^{K}$ and update the values of p_k for each $k = 1, 2, \ldots, K$ until convergence. Thus, we have an algorithm to compute $\{p_k\}_{k=1}^{K}$ if $\mathbf{U}$ is known, which is summarized in Algorithm 6. The whole procedure for evaluating $\mathbf{F}$ is summarized in Algorithm 7.

VI. Solution for Sensing Signal

A. Projection of sensing signal into the null space of communication channel

We need to make sure $\mathbf{s}_r$ lies in the null space of the channel matrix $\mathbf{H}$. If $\tilde{\mathbf{x}} = \tilde{\mathbf{s}}_\mathbf{r} + \mathbf{F}\mathbf{s}_c$ is the solution to the problem (11), it can be achieved by projecting $\tilde{\mathbf{s}}_\mathbf{r}$ in the null space of $\mathbf{H}$. But we need to make sure that the power of the resulting signal does not exceed the available power for sensing, which is $P_T - P_c$. Thus, the resulting sensing signal can be expressed as

$$\mathbf{s}_r = P_r \frac{\mathcal{N}_{\text{H}} \tilde{\mathbf{s}}_\mathbf{r}}{\|\mathcal{N}_{\text{H}} \tilde{\mathbf{s}}_\mathbf{r}\|}, \tag{39}$$

where $\mathcal{N}_{\text{H}} \triangleq \mathbf{V}_0 \mathbf{V}_0^H$ is the null space of $\mathbf{H}$, $\mathbf{V}_0 \in \mathbb{C}^{N_t \times b}$ is the matrix consisting of right singular vectors of $\mathbf{H}$ corresponding to zero singular values and $b = N_t - \text{rank}(\mathbf{H})$ and P_r is the adjustable sensing power such that $P_r \leq P_T - P_c$. We assume that users are spatially separated so that the channels to different users are uncorrelated in which case $\text{rank}(\mathbf{H}) = K$. However, we aim to simplify the problem. To this end, we force $\mathbf{s}_r$ to lie in the null space of $\mathbf{H}$ by defining $\mathbf{s}_r \triangleq \mathcal{N}_{\text{H}} \bar{\mathbf{s}}_\mathbf{r}$ where $\bar{\mathbf{s}}_\mathbf{r} \in \mathbb{C}^{N_t \times 1}$.

B. Computation of sensing signal

We solve the optimization problem

$$\min_{\bar{\mathbf{s}}_r} \quad \left\|\mathbf{d} - \bar{\mathbf{A}}\bar{\mathbf{s}}_r - \mathbf{A}\mathbf{F}\mathbf{s}_c\right\|^2 \tag{40a}$$

$$s.t. \quad |\bar{s}_{s_m}| = \sqrt{\frac{P_T - P_c}{N_t}}, \quad m = 1, 2, \ldots, N_t, \tag{40b}$$

where $\bar{\mathbf{A}} = \mathbf{A}\mathcal{N}_{\text{H}}$. The objective function in (40a) can simplified as

$$\begin{aligned}&\left\|\mathbf{d}-\bar{\mathbf{A}}\bar{\mathbf{s}}_r-\mathbf{A}\mathbf{F}\mathbf{s}_c\right\|^2\\=&\bar{\mathbf{s}}_r^H\bar{\mathbf{A}}^H\bar{\mathbf{A}}\bar{\mathbf{s}}_r-\mathbf{d}^H\bar{\mathbf{A}}\bar{\mathbf{s}}_r-\bar{\mathbf{s}}_r^H\bar{\mathbf{A}}^H\mathbf{d}+\|\mathbf{A}\mathbf{F}\|_F^2-\\&2\Re\left(\mathbf{d}^H\mathbf{A}\mathbf{F}\mathbf{s}_c\right)+\mathbf{d}^H\mathbf{d}\\=&\bar{\mathbf{s}}_r^H\mathbf{G}\bar{\mathbf{s}}_r-\mathbf{q}^H\bar{\mathbf{s}}_r-\bar{\mathbf{s}}_r^H\mathbf{q}+c,\end{aligned}$$

where $\mathbf{G} \triangleq \bar{\mathbf{A}}^H\bar{\mathbf{A}}, \mathbf{q} \triangleq \mathbf{d}^H\bar{\mathbf{A}}$ and $c \triangleq \mathbf{d}^H\mathbf{d} + \|\mathbf{A}\mathbf{F}\|_F^2 - 2\Re\left(\mathbf{d}^H\mathbf{A}\mathbf{F}\mathbf{s}_c\right)$. Thus, the optimization problem (40) can be rewritten as

$$\min_{\bar{\mathbf{s}}_r} \quad \bar{\mathbf{s}}_r^H\mathbf{G}\bar{\mathbf{s}}_r-\mathbf{q}^H\bar{\mathbf{s}}_r-\bar{\mathbf{s}}_r^H\mathbf{q}+c \tag{41a}$$

$$s.t. \quad |\bar{s}_{s_m}| = \sqrt{\frac{P_T-P_c}{N_t}}, \quad m=1,2,\ldots,N_t, \tag{41b}$$

The problem in (42) is similar to the passive beamforming subproblem based on minimum mean square error (MMSE) in [48]. Taking a similar route, the optimization problem in (42) can be written equivalently as

$$\min_{\bar{\mathbf{s}}_r} \quad \bar{\mathbf{s}}_r^H\left(\mathbf{G}+\mu\mathbf{I}\right)\bar{\mathbf{s}}_r-\mathbf{q}^H\bar{\mathbf{s}}_r-\bar{\mathbf{s}}_r^H\mathbf{q} \tag{42a}$$

$$s.t. \quad |\bar{s}_{r_m}| = \sqrt{\frac{P_T-P_c}{N_t}}, \quad m=1,2,\ldots,N_t, \tag{42b}$$

where $\mu = \dfrac{c}{N_t}$. In the absence of the constraint (42b), the optimal solution to the problem (40) would be $\bar{\mathbf{s}}_r^{uc} = \left(\mathbf{G}+\mu\mathbf{I}\right)^{-1}\mathbf{q}$. Thus, in order to determine $\bar{\mathbf{s}}_r$, we normalize each element of $\bar{\mathbf{s}}_r^{uc}$ to have an amplitude $\sqrt{\dfrac{P_T-P_c}{N_t}}$,

$$\bar{\mathbf{s}}_r = \sqrt{\frac{P_T-P_c}{N_t}}\exp\left(j\angle\left(\left(\mathbf{G}+\mu\mathbf{I}\right)^{-1}\mathbf{q}\right)\right) \tag{43}$$

Then, we compute $\mathbf{s}_r$ from $\bar{\mathbf{s}}_r$ using (39).

C. Sensing signal power

The received echo signal is passed through a receive beamformer $\mathbf{W} = [\mathbf{w}_1, \ldots, \mathbf{w}_Q]$ where $\mathbf{w}_q, \ q = 1, \ldots, Q$ is the receive beamformer for q^{th} target. The beamformer $\mathbf{w}_q$ is designed to maximize the received power,

$$\max_{\mathbf{w}_q} \quad \left\|\mathbf{w}_q^H\left(\alpha_q\mathbf{b}\left(\theta_q\right)\mathbf{a}\left(\theta_q\right)^H\mathbf{x}\right)\right\|^2 \tag{44}$$

The optimal $\mathbf{w}_q$ is given by $\mathbf{b}\left(\theta_q\right)$ [25]. We determine the sensing power P_r so that individual sensing SINR is met for each target, *i.e.*, the optimization problem to determine P_r is formulated as

$$\text{Find} \quad P_r \tag{45a}$$

$$s.t. \frac{\tau_q\left\|\mathbf{w}_q^H\mathbf{b}\left(\theta_q\right)\mathbf{a}\left(\theta_q\right)^H\mathbf{x}\right\|^2}{\sum\limits_{j=1,j\neq q}^{Q}\tau_j\left\|\mathbf{w}_q^H\mathbf{b}\left(\theta_j\right)\mathbf{a}\left(\theta_j\right)^H\mathbf{x}\right\|^2+\sigma_r^2} \geq \zeta_q, \tag{45b}$$

where ζ_q is the sensing SINR target for the q^{th} target. We assume that the required sensing SINR can be achieved by available power $P_T - P_c$. P_r is thus calculated as

$$P_r = \max_q \tag{46}$$

$$\frac{\zeta_q\sum\limits_{j\neq q}^{Q}\tau_j\left\|\mathbf{w}_q^H\mathbf{b}\left(\theta_j\right)\mathbf{a}\left(\theta_j\right)^H\mathbf{F}\right\|^2-N_r^2\tau_q\left\|\mathbf{a}\left(\theta_q\right)^H\mathbf{F}\right\|^2+\zeta_q\sigma_r^2}{N_r^2\tau_q\left|\mathbf{a}\left(\theta_q\right)^H\mathbf{s}_r\right|^2-\zeta_q\sum\limits_{j\neq q}^{Q}\tau_j\left|\mathbf{w}_q^H\mathbf{b}\left(\theta_j\right)\mathbf{a}\left(\theta_j\right)^H\mathbf{s}_r\right|^2},$$

where $\mathbf{w}_q^H\mathbf{b}\left(\theta_q\right), i = 1, \ldots, T$ is replaced by N_r. The sensing signal is normalized and multiplied by P_r to have the power P_r.

VII. Complexity of the proposed algorithms

We compute the complexity of various algorithms by calculating the computational complexities of the dominant operations in each of the algorithms.

1) Alternating Optimization-based Solution for Communication Signal:
   - Complexity in solving SOCP (14) : $\mathcal{O}\left(\sqrt{K}\left(KN_t\right)^3\log\left(\frac{1}{\epsilon}\right)\right)$ [36], where ϵ is solution accuracy.
   - Complexity in Feasibility-check problem (16): It is an SDP which has a computational complexity of $\mathcal{O}\left(K^3M^6\right)$ [49]. During each iteration of alternating optimization, it is repeated I_F times on average leading to a complexity of $\mathcal{O}\left(I_FK^3M^6\right)$.

   Thus, the total complexity of alternating optimization-based solution is $\mathcal{O}\left(I_a\left(\sqrt{K}\left(KN_t\right)^3\log\left(\frac{1}{\epsilon}\right)+I_FK^3M^6\right)\right)$, where I_a is the number of iterations.
2) Two-stage Solution for Communication Signal:

   2.1. Passive Beamforming
   - Complexity in cost function computation: $\mathcal{O}\left(M^2\right)$
   - Complexity in gradient computation: $\mathcal{O}\left(M^2\right)$
   - Complexity in Manifold Optimization: $\mathcal{O}\left(I_{m_1}M^2\right)$ where I_{m_1} is the number of iterations required.

   2.2. Precoding
   - Complexity in cost function computation: $\mathcal{O}\left(K^2M\right)$
   - Complexity in gradient computation: $\mathcal{O}\left(K^2M\right)$
   - Complexity in Manifold Optimization: $\mathcal{O}\left(I_{m_2}K^2M\right)$ where I_{m_2} is the number of iterations required.
   - Complexity in Power Allocation Computation: $\mathcal{O}\left(K^2M+I_pK^2\right)$ where I_p is number of iterations required to reach convergence.

   The overall complexity of the two-stage solution for communication signal is $\mathcal{O}\left(I_{m_1}M^2+I_{m_2}K^2M+I_pK^2\right)$.
3) Sensing Signal: The main complexity comes from the computation of inverse matrix of a $N_t \times N_t$ matrix which is $\mathcal{O}\left(N_t^3\right)$ [48].

Hence, the complexity of waveform design with alternating optimization for communication signal is $\mathcal{O}\left(I_a\left(\sqrt{K}\left(KN_t\right)^3\log\left(\frac{1}{\epsilon}\right)+I_FK^3M^6\right)+N_t^3\right)$, whereas that of manifold optimization based solution is $\mathcal{O}\left(I_{m_1}M^2+I_{m_2}K^2M+I_pK^2+N_t^3\right)$. The complexity of manifold optimization based waveform design is much lower than the complexity of state-of-the-art solution [30] which is $\mathcal{O}\left(I_o\left(KN_t^2+K^3M^6\right)+N_t^{4.5}\right)$ where I_o is the number of iterations.

VIII. Simulation Results

We consider an ISAC MIMO system with a single BS, a single RIS assisting communication with K single-antenna UEs and Q sensing targets. The BS and RIS are located at $(0,0,0)$ and $(36,36,0)$. All the UEs are placed on the semicircle of radius $5m$ centered at $(40,15,0)$. The exact placement of the UEs, however, is chosen randomly. The top view of the placement of BS, RIS, and UEs is illustrated in the Fig.2. The distance-dependent path loss model is adopted, which is given by

$$L\left(d\right)=K_0\left(\frac{d}{D_0}\right)^{-\zeta} \tag{47}$$

where K_0 is the path loss at the reference distance D_0 = 1 m, d denotes the individual link distance, and ζ denotes the path loss exponent. We consider the Rician fading channel model for all the channels to account for small-scale fading. The BS-RIS channel and RIS-k^{th}user channel are respectively given by

$$\mathbf{H}_{BR}=L\left(d_{BR}\right)\left(\sqrt{\frac{\kappa_{BR}}{\kappa_{BR}+1}}\mathbf{H}_{BR,L}+\sqrt{\frac{1}{\kappa_{BR}+1}}\mathbf{H}_{BR,NL}\right), \tag{48a}$$

where

$$\mathbf{H}_{BR,L}=\left(\mathbf{a}\left(\phi_{B,d}\right)\mathbf{a}_R^H\left(\phi_{R,a}\right)\right)^T, \tag{48b}$$

$$h_{BR,NL}^{m,n}\sim\mathcal{CN}\left(0,1\right),\ m=1,\ldots,M;\ n=1,\ldots,N_t \tag{48c}$$

$$\mathbf{h}_{R,k}=L\left(d_{RU,k}\right)\left(\sqrt{\frac{\kappa_R}{\kappa_R+1}}\mathbf{h}_{R_k,L}+\sqrt{\frac{1}{\kappa_R+1}}\mathbf{h}_{R_k,NL}\right),\quad\forall\ k \tag{49a}$$

where

$$\mathbf{h}_{R_k,L}=\mathbf{a}_R\left(\phi_{R,d}\right)^T, \tag{49b}$$

$$h_{R_k,NL}^i\sim\mathcal{CN}\left(0,1\right),\ i=1,\ldots,M, \tag{49c}$$

in which d_{BR} and $d_{RU,k}$ are the BS-RIS and RIS-k^{th}user link distances respectively, whereas $h_{BR,NL}^{m,n}$ and $h_{R_k,NL}^i$ are $(m,n)^{th}$ entry of $H_{BR,NL}$ and i^{th} entry of $h_{R_k,NL}$ respectively. For simulations, we take K_0 = -30 dB, $\kappa_{BR}=2$, $\kappa_R=2.8$, and $\zeta=$ 2.5 and 3.5 for BS-user and BS-RIS links, respectively.

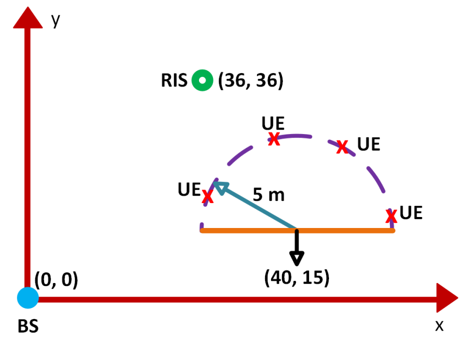

Fig. 2: Top view of the placement of BS, RIS, and UEs.

The BS is assumed to be equipped with a uniform linear array (ULA) having N_t antennas, whereas the RIS utilizes a uniform planar array (UPA) with $M=M^y\times M^z$ antennas. All antenna elements are separated by a distance of half a wavelength. The noise power $\sigma_c^2=-117$ dBm. Minimum SINR constraints for all the users are considered equal, *i.e.*, $\gamma_k=\gamma,\ \forall k=1,\ldots,K$. The typical values of all the parameters used in simulations are given in Table I.

TABLE I: PARAMETERS FOR SIMULATIONS

Parameters	N_t	M	K	σ_c^2	γ_k	P_{max}
Values	16	25	4	-117 dBm	20 dBm	35 dBm

We summarize implementation details for both AO and manifold-based methods in Table II and Table III respectively.

TABLE II: ALGORITHM PARAMETERS FOR AO-BASED METHOD

Parameter	**Value**
	Algorithm 1
$\mathbf{\Phi}^{(0)}$	Random Phase angles from uniform distribution
ϵ_{tol}	10^{-7}
$iter_{max}$	10
cvx precision	1.49e-08
	Algorithm 2
γ_k	γ_{min}
ν_{min}, ν_{max}	γ_{min}, $2\gamma_{min}$
ϵ_{tol}	10^{-3}
cvx precision	1.49e-08

TABLE III: ALGORITHM PARAMETERS FOR MO-BASED METHOD

Parameter	**Value**
	Algorithms 4,5,6
ϵ_{tol}	10^{-3} (Alg. 6), 10^{-6} (Alg. 4,5)
	Algorithm 7
$p_k^{(0)}$	$\sigma_c^2\gamma_k$, where $\gamma_k=\gamma_{min},\forall k=1,\ldots,K$
ϵ_{tol}	10^{-3}
	Manopt parameters
maxiter	100
tolgradnorm	10^{-8} (Alg. 5), 10^{-6} (Alg. 4)

We compare the communication performances of the proposed methods with conventional ZF/MMSE precoders and the existing solution [30]. In the figures, the proposed alternating optimization-based algorithm is labeled **P-AO**, while **ZF** refers to the ZF precoding-based solution, **MMSE** refers to the MMSE precoding-based solution, and **Existing** refers to the state-of-the-art solution based on the algorithm in [30]. In the simulations, **Existing** uses a tolerance of 10^{-4} throughout, initializes RIS with the phase angles drawn from a uniform distribution, and makes the rank-1 approximation of the SDP solution via the dominant SVD vector. There are no step size involved in the existing algorithm. ZF precoder is computed as

$$\mathbf{F}_{ZF} = \mathbf{H}^H \left(\mathbf{H}^H\mathbf{H}\right)^{-1} \mathrm{DIAG}\left(\sqrt{\gamma_1 \sigma_c^2}, \dots, \sqrt{\gamma_K \sigma_c^2}\right) \quad (50)$$

On the other hand, the MMSE precoder is computed as

$$\mathbf{F}_{MMSE} = \left(\mathbf{H}\mathbf{P}_{MMSE}^{-1/2}\mathbf{H}^H + \sigma_c^2\mathbf{I}\right)^{-1}\mathbf{H}^H, \quad (51)$$

where $\mathbf{P}_{MMSE} = \mathrm{DIAG}\left(\gamma_1\sigma_c^2, \dots, \gamma_K\sigma_c^2\right)$. **P-MO (random Φ)** in the figures represents the solution that uses random initialization of RIS phase-shifts followed by manifold optimization-based algorithm in Algorithm 5, whereas **P-MO (2-stage)** refers to the proposed manifold optimization-based two-stage algorithm to compute communication signal in Algorithm 7. The performance gap between **P-MO (random Φ)** and **P-MO (2-stage)** is used to highlight the efficacy of the proposed passive beamforming solution in Algorithm 4.

We first show the complexity of both the proposed algorithms, along with the existing method in terms of average runtime in Fig.3. All the algorithms are executed in MATLAB 2023a on a personal computer with 11^{th} Gen Intel Core i7 2.8 GHz processor and 16 GB RAM. It is evident that both **P-AO** and **Existing** are computationally expensive, with **P-AO** having even more computational complexity. However, **P-MO** is highly computationally efficient.

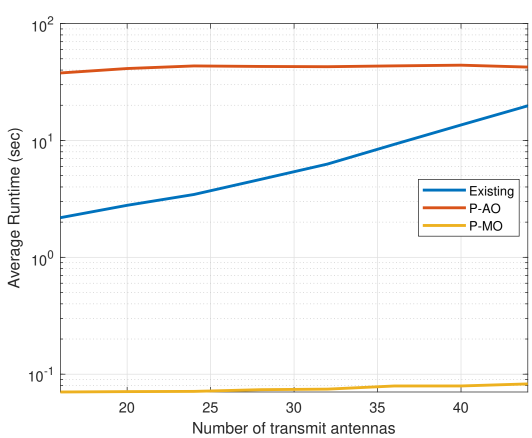

Fig. 3: Average run-time vs. Number of transmit antennas

A. Communication Performance

In Fig.4, Fig.5 and Fig.6, we observe how the communication transmit power behaves as the minimum SINR constraint,

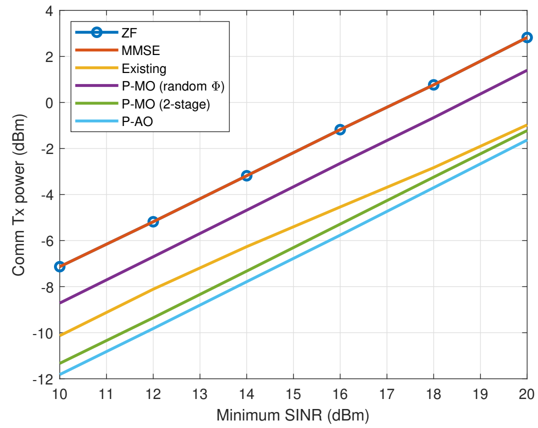

Fig. 4: Communication Transmit Power vs. SINR

the number of RIS elements M and the number of transmit antennas N_t are varied. When the minimum SINR constraint for each user increases, there is an increase in communication transmit power, which is natural as more power is required to furnish a higher SINR for each user. In Fig.5, we can see that the communication transmit power decreases with the increasing number of RIS elements for a fixed minimum SINR constraint, as the increasing RIS elements furnish more passive beamforming gain. The transmit communication power curves exhibit similar behavior in Fig.6 as the number of transmit antennas increases. This is due to higher antenna gain, which reduces the transmit power needed to maintain the required SINR.

The conventional ZF and MMSE precoders perform the worst as they require the highest power among all the compared methods to deliver the same values of SINR. In each of the Fig.4, Fig.5 and Fig.6, we can observe that there is a huge difference in transmit communication power between ZF/MMSE and P-MO (random Φ). Since ZF, MMSE, and P-MO (random Φ) all use random phase-shifts of RIS, the better power-efficiency of P-MO (random Φ) shows the superiority of the proposed Algorithm 7) in determining the minimum-power precoder. Moreover, P-MO (2-stage) is more power-efficient than P-MO (random Φ), which affirms the effectiveness of the passive beamforming algorithm in Algorithm 4. Overall, the proposed P-AO and P-MO deliver better power efficiency performance, compared to the existing method, with P-AO coming out as the best. Furthermore, we can observe that the performance gap between the existing and proposed methods narrows at higher SINR values but widens at higher numbers of RIS elements and transmit antennas.

B. Sensing Performance

In this section, we compare the sensing performance of the proposed method with that of the existing one. **P-MO (FP)**, **P-MO (10 dBm)** and **P-MO (15 dBm)** in the figures represent proposed method with full sensing power, sensing SINR 10

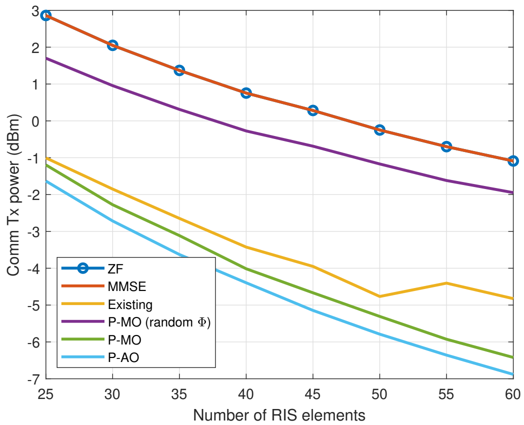

Fig. 5: Communication Transmit Power vs. Number of RIS elements

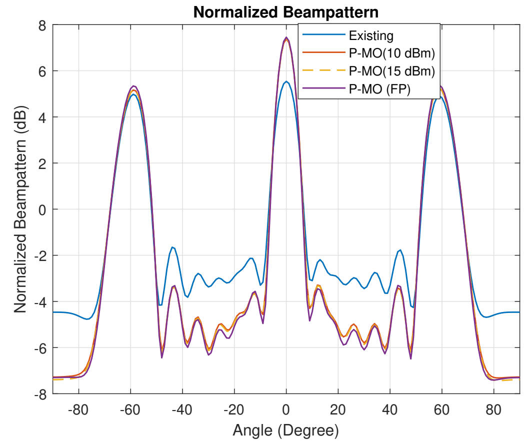

Fig. 7: Normalized Beampattern of the ISAC signal vs. Angle, Target location = $-60°,\ 0°,\ 60°$

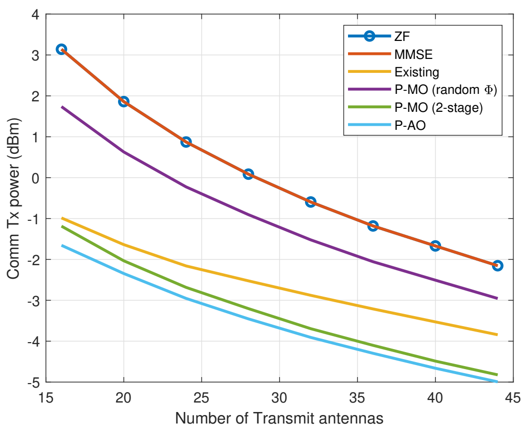

Fig. 6: Communication Transmit Power vs. Number of transmit antennas

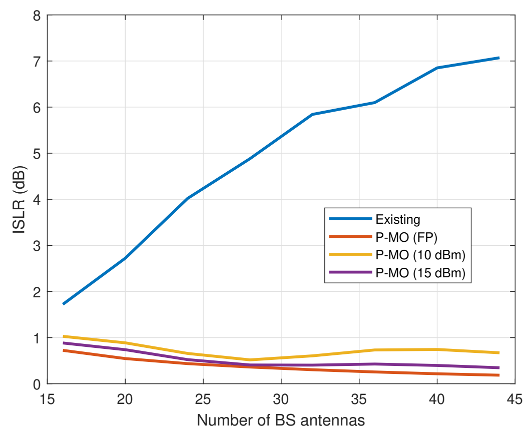

Fig. 8: ISLR vs. Number of BS antennas, Target location = 0°

dBm and sensing SINR 15 dBm respectively. The desired beampattern is given by

$$d(\theta) = \begin{cases} 1,\ \theta = [\theta_{T_1} - 5°, \theta_{T_1} + 5°], \dots, \\ \qquad [\theta_{T_Q} - 5°, \theta_{T_Q} + 5°] \\ 0,\ otherwise, \end{cases} \tag{52}$$

where $\theta_{T_q},\ q = 1, \dots, Q$ refers to target location in terms of angle and Q is the number of targets. In Fig.7, the normalized beampattern of the radar sensing signal of the proposed method is compared with that of the existing one when the number of targets is 3. From this figure, it is clear that the proposed sensing signal has higher illumination at the target locations compared to the existing sensing signal. On the other hand, the proposed sensing signal has less normalized power than the existing sensing signal at angles different from the target locations. This is further proved by Fig.8, where we compare the integrated-sidelobe ratio (ISLR) of the proposed and existing sensing signals as the number of BS antennas is varied. A lower ISLR value is desirable because it implies that the effective interference seen by any target at a given angle is low, which directly raises the sensing SINR. The proposed method clearly achieves better ISLR compared to the existing method. In Fig.9, we plot the probability of detection vs. the probability of false alarm. The detection statistic is constructed from the matched-filter output aligned with the target steering vector, and the corresponding detection threshold is determined empirically from noise-only realizations for each probability of false alarm. The proposed method with full power performs better than all, including the existing method.

The Fig.10 compares the total power of the proposed waveform with the existing waveform as the communication SINR varies. The existing waveform uses all available transmit power, while the proposed waveform uses only the power needed to maintain a minimum sensing SINR at the receiver, thereby utilizing the power efficiently.

IX. Conclusion

This paper explores an ISAC system where a Reconfigurable Intelligent Surface (RIS) enhances communication. We propose designing an ISAC signal that optimizes power-efficient

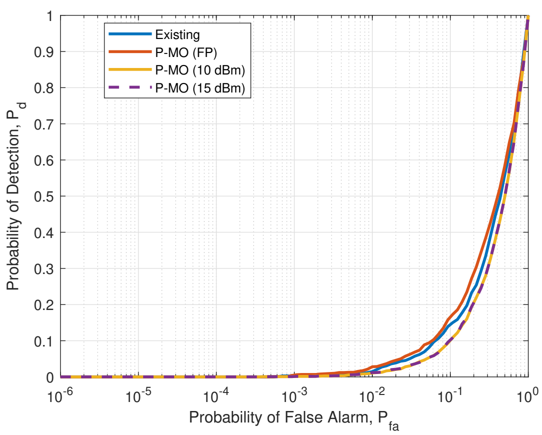

Fig. 9: Probability of detection vs. Probability of false alarm

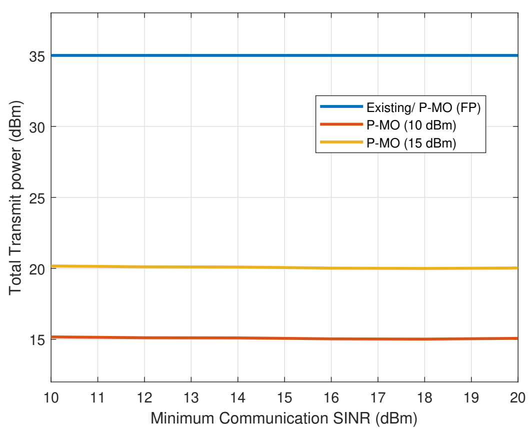

Fig. 10: Total power vs. Minimum Communication SINR

communication, freeing up most transmit power for sensing. The RIS establishes communication channels between the BS and the users. The RIS is jointly optimized with transmit precoding to leverage a beamforming gain to help achieve the required SINR target for all users. We introduce an alternating optimization algorithm that alternately determines transmit precoding and the passive beamforming until convergence. Additionally, we propose a two-stage algorithm where we initially optimize passive beamforming and then design transmit precoding, employing manifold optimization. The sensing signal is designed to minimize the difference between the beam pattern of the ISAC waveform and the desired beam pattern. Finally, the sensing signal is projected on the null space of the communication channel to cancel its effect on the communication signal.

Appendix A

If $\lambda_1 \geq \lambda_2 \geq \cdots \geq \lambda_r > 0,\ 0 < r \leq n$ are the r non-zero singular values of a positive semidefinite matrix $\mathbf{A} \in \mathbb{C}^{n\times n}$ with rank r, the singular values of its pseudoinverse $\mathbf{A}^\dagger$ are $0 < \lambda_1^{-1} \leq \lambda_2^{-1} \leq \cdots \leq \lambda_r^{-1}$. We can express the trace of $\mathbf{A}$ and trace of $\mathbf{A}^\dagger$ as

$$\mathbf{Tr}\left(\mathbf{A}\right) = \sum_{i=1}^{r} \lambda_i \tag{53a}$$

$$\mathbf{Tr}\left(\mathbf{A}^\dagger\right) = \sum_{i=1}^{r} \lambda_i^{-1}. \tag{53b}$$

The product of trace of $\mathbf{A}$ and trace of $\mathbf{A}^\dagger$ is

$$\mathbf{Tr}\left(\mathbf{A}\right)\mathbf{Tr}\left(\mathbf{A}^\dagger\right) = \left(\sum_{i=1}^{r} \lambda_i\right)\left(\sum_{i=1}^{r} \lambda_i^{-1}\right). \tag{54}$$

Since $\lambda_1, \lambda_2, \ldots, \lambda_r$ is a non-increasing sequence, and $\lambda_1^{-1}, \lambda_2^{-1}, \ldots, \lambda_r^{-1}$ is a non-decreasing sequence, we can write

$$\begin{aligned}\left(\sum_{i=1}^{r} \lambda_i\right)\left(\sum_{i=1}^{r} \lambda_i^{-1}\right) &\geq r\sum_{i=1}^{r} \lambda_i\lambda_i^{-1} \\ &= r^2,\end{aligned}$$

using Chebyshev inequality [50]. The equality is fulfilled when $\lambda_1 = \lambda_2 = \cdots = \lambda_r$. Hence,

$$\mathbf{Tr}\left(\mathbf{A}\right)\mathbf{Tr}\left(\mathbf{A}^\dagger\right) \geq r^2. \tag{55}$$

Since $\mathbf{Tr}\left(\mathbf{A}\right) > 0$, we may express the trace of $\mathbf{A}^\dagger$ as

$$\mathbf{Tr}\left(\mathbf{A}^\dagger\right) \geq \frac{r^2}{\mathbf{Tr}\left(\mathbf{A}\right)}, \tag{56}$$

with equality when all the singular values of $\mathbf{A}$ are equal.

References

[1] R. Saruthirathanaworakun, J. M. Peha, and L. M. Correia, “Opportunistic sharing between rotating radar and cellular,” *IEEE Journal on Selected Areas in Communications*, vol. 30, no. 10, pp. 1900–1910, 2012.

[2] ——, “Opportunistic primary-secondary spectrum sharing with a rotating radar,” in *2012 International Conference on Computing, Networking and Communications (ICNC)*, 2012, pp. 1025–1030.

[3] J. Moghaddasi and K. Wu, “Multifunctional transceiver for future radar sensing and radio communicating data-fusion platform,” *IEEE Access*, vol. 4, pp. 818–838, 2016.

[4] S. Sodagari, A. Khawar, T. C. Clancy, and R. McGwier, “A projection based approach for radar and telecommunication systems coexistence,” in *2012 IEEE Global Communications Conference (GLOBECOM)*, 2012, pp. 5010–5014.

[5] A. Khawar, A. Abdelhadi, and C. Clancy, “Target detection performance of spectrum sharing mimo radars,” *IEEE Sensors Journal*, vol. 15, no. 9, pp. 4928–4940, 2015.

[6] A. Khawar, A. Abdelhadi, and T. C. Clancy, “Coexistence analysis between radar and cellular system in los channel,” *IEEE Antennas and Wireless Propagation Letters*, vol. 15, pp. 972–975, 2016.

[7] J. A. Mahal, A. Khawar, A. Abdelhadi, and T. C. Clancy, “Spectral coexistence of mimo radar and mimo cellular system,” *IEEE Transactions on Aerospace and Electronic Systems*, vol. 53, no. 2, pp. 655–668, 2017.

[8] F. Liu, Y.-F. Liu, A. Li, C. Masouros, and Y. C. Eldar, “Cramér-rao bound optimization for joint radar-communication beamforming,” *IEEE Transactions on Signal Processing*, vol. 70, pp. 240–253, 2022.

[9] X. Liu, T. Huang, N. Shlezinger, Y. Liu, J. Zhou, and Y. C. Eldar, “Joint transmit beamforming for multiuser mimo communications and mimo radar,” *IEEE Transactions on Signal Processing*, vol. 68, pp. 3929–3944, 2020.

[10] R. M. Mealey, “A method for calculating error probabilities in a radar communication system,” *IEEE Transactions on Space Electronics and Telemetry*, vol. 9, no. 2, pp. 37–42, 1963.

[11] A. Hassanien, M. G. Amin, Y. D. Zhang, and F. Ahmad, "Dual-function radar-communications: Information embedding using sidelobe control and waveform diversity," *IEEE Transactions on Signal Processing*, vol. 64, no. 8, pp. 2168–2181, 2016.

[12] ——, "Phase-modulation based dual-function radar-communications," *IET Radar, Sonar & Navigation*, vol. 10, no. 8, pp. 1411–1421, 2016.

[13] X. Wang, A. Hassanien, and M. G. Amin, "Sparse transmit array design for dual-function radar communications by antenna selection," *Digital Signal Processing*, vol. 83, pp. 223–234, 2018.

[14] A. Hassanien, E. Aboutanios, M. G. Amin, and G. A. Fabrizio, "A dual-function mimo radar-communication system via waveform permutation," *Digital Signal Processing*, vol. 83, pp. 118–128, 2018.

[15] X. Wang, A. Hassanien, and M. G. Amin, "Dual-function mimo radar communications system design via sparse array optimization," *IEEE Transactions on Aerospace and Electronic Systems*, vol. 55, no. 3, pp. 1213–1226, 2019.

[16] M. Roberton and E. Brown, "Integrated radar and communications based on chirped spread-spectrum techniques," in *IEEE MTT-S International Microwave Symposium Digest, 2003*, vol. 1, 2003, pp. 611–614 vol.1.

[17] G. N. Saddik, R. S. Singh, and E. R. Brown, "Ultra-wideband multifunctional communications/radar system," *IEEE Transactions on Microwave Theory and Techniques*, vol. 55, no. 7, pp. 1431–1437, 2007.

[18] A. Hassanien, M. G. Amin, Y. D. Zhang, and B. Himed, "A dual-function mimo radar-communications system using psk modulation," in *2016 24th European Signal Processing Conference (EUSIPCO)*, 2016, pp. 1613–1617.

[19] D. Ma, T. Huang, Y. Liu, and X. Wang, "A novel joint radar and communication system based on randomized partition of antenna array," in *2018 IEEE International Conference on Acoustics, Speech and Signal Processing (ICASSP)*, 2018, pp. 3335–3339.

[20] T. Huang, N. Shlezinger, X. Xu, Y. Liu, and Y. C. Eldar, "Majorcom: A dual-function radar communication system using index modulation," *IEEE Transactions on Signal Processing*, vol. 68, pp. 3423–3438, 2020.

[21] C. Sturm, T. Zwick, and W. Wiesbeck, "An ofdm system concept for joint radar and communications operations," in *VTC Spring 2009 - IEEE 69th Vehicular Technology Conference*, 2009, pp. 1–5.

[22] C. Sturm and W. Wiesbeck, "Waveform design and signal processing aspects for fusion of wireless communications and radar sensing," *Proceedings of the IEEE*, vol. 99, no. 7, pp. 1236–1259, 2011.

[23] F. Liu, C. Masouros, A. Li, H. Sun, and L. Hanzo, "Mu-mimo communications with mimo radar: From co-existence to joint transmission," *IEEE Transactions on Wireless Communications*, vol. 17, no. 4, pp. 2755–2770, 2018.

[24] F. Liu, L. Zhou, C. Masouros, A. Li, W. Luo, and A. Petropulu, "Toward dual-functional radar-communication systems: Optimal waveform design," *IEEE Transactions on Signal Processing*, vol. 66, no. 16, pp. 4264–4279, 2018.

[25] Z. He, W. Xu, H. Shen, Y. Huang, and H. Xiao, "Energy efficient beamforming optimization for integrated sensing and communication," *IEEE Wireless Communications Letters*, vol. 11, no. 7, pp. 1374–1378, 2022.

[26] A. Bazzi and M. Chafii, "On integrated sensing and communication waveforms with tunable papr," *IEEE Transactions on Wireless Communications*, vol. 22, no. 11, pp. 7345–7360, 2023.

[27] ——, "Low dynamic range for ris-aided bistatic integrated sensing and communication," *IEEE Journal on Selected Areas in Communications*, vol. 43, no. 3, pp. 912–927, 2025.

[28] Z. He, W. Xu, H. Shen, D. W. K. Ng, Y. C. Eldar, and X. You, "Full-duplex communication for isac: Joint beamforming and power optimization," *IEEE Journal on Selected Areas in Communications*, vol. 41, no. 9, pp. 2920–2936, 2023.

[29] H. Hua, J. Xu, and T. X. Han, "Optimal transmit beamforming for integrated sensing and communication," *IEEE Transactions on Vehicular Technology*, vol. 72, no. 8, pp. 10 588–10 603, 2023.

[30] J. Chen, K. Wu, J. Niu, Y. Li, P. Xu, and J. Andrew Zhang, "Spectral and energy efficient waveform design for ris-assisted isac," *IEEE Transactions on Communications*, vol. 73, no. 1, pp. 158–172, 2025.

[31] Y. Xiu, W. Lyu, P. L. Yeoh, Y. Ai, and N. Wei, "Secure enhancement for ris-aided aav with isac: Robust design and resource allocation," *IEEE Transactions on Vehicular Technology*, vol. 75, no. 4, pp. 6776–6791, 2026.

[32] Y. Xiu, S. Yang, W. Lyu, P. Lep Yeoh, Y. Li, and Y. Ai, "Movable antenna enabled isac beamforming design for low-altitude airborne vehicles," *IEEE Wireless Communications Letters*, vol. 14, no. 5, pp. 1311–1315, 2025.

[33] Y. Xiu, Y. Zhao, R. Yang, D. Niyato, J. Jin, Q. Wang, G. Liu, and N. Wei, "Movable antenna-aided cooperative isac network with time synchronization error and imperfect csi," *IEEE Transactions on Communications*, vol. 74, pp. 2968–2983, 2026.

[34] H. He, P. Stoica, and J. Li, "Wideband mimo systems: Signal design for transmit beampattern synthesis," *IEEE Transactions on Signal Processing*, vol. 59, no. 2, pp. 618–628, 2011.

[35] K. Alhujaili, V. Monga, and M. Rangaswamy, "Transmit mimo radar beampattern design via optimization on the complex circle manifold," *IEEE Transactions on Signal Processing*, vol. 67, no. 13, pp. 3561–3575, 2019.

[36] Z.-Q. Luo and W. Yu, "An introduction to convex optimization for communications and signal processing," *IEEE Journal on Selected Areas in Communications*, vol. 24, no. 8, pp. 1426–1438, 2006.

[37] I. CVX Research, "CVX: Matlab software for disciplined convex programming, version 2.0," http://cvxr.com/cvx, Aug. 2012.

[38] G. Caire and S. Shamai, "On the achievable throughput of a multiantenna gaussian broadcast channel," *IEEE Transactions on Information Theory*, vol. 49, no. 7, pp. 1691–1706, 2003.

[39] A. Wiesel, Y. C. Eldar, and S. Shamai, "Zero-forcing precoding and generalized inverses," *IEEE Transactions on Signal Processing*, vol. 56, no. 9, pp. 4409–4418, 2008.

[40] E. Björnson, M. Bengtsson, and B. Ottersten, "Optimal multiuser transmit beamforming: A difficult problem with a simple solution structure [lecture notes]," *IEEE Signal Processing Magazine*, vol. 31, no. 4, pp. 142–148, 2014.

[41] P. R. Gautam, L. Zhang, and P. Fan, "Hybrid MMSE precoding for millimeter wave MU-MISO via trace maximization," *IEEE Transactions on Wireless Communications*, vol. 23, no. 3, pp. 1999–2010, 2024.

[42] M. Soltanalian and P. Stoica, "Designing unimodular codes via quadratic optimization," *IEEE Transactions on Signal Processing*, vol. 62, no. 5, pp. 1221–1234, 2014.

[43] J. M. Lee and J. M. Lee, *Smooth manifolds*. Springer, 2003.

[44] X. Yu, J.-C. Shen, J. Zhang, and K. B. Letaief, "Alternating minimization algorithms for hybrid precoding in millimeter wave mimo systems," *IEEE Journal of Selected Topics in Signal Processing*, vol. 10, no. 3, pp. 485–500, 2016.

[45] P.-A. Absil, R. Mahony, and R. Sepulchre, "Optimization algorithms on matrix manifolds," in *Optimization Algorithms on Matrix Manifolds*. Princeton University Press, 2009.

[46] Y. Ma and Y. Fu, *Manifold learning theory and applications*. CRC press Boca Raton, 2012, vol. 434.

[47] N. Boumal, B. Mishra, P.-A. Absil, and R. Sepulchre, "Manopt, a matlab toolbox for optimization on manifolds," *The Journal of Machine Learning Research*, vol. 15, no. 1, pp. 1455–1459, 2014.

[48] P. R. Gautam, L. Zhang, and P. Fan, "MMSE-based passive beamforming for reconfigurable intelligent surface aided millimeter wave MIMO," *IET Communications*, vol. 19, no. 1, p. e12873, 2025.

[49] Z.-q. Luo, W.-k. Ma, A. M.-c. So, Y. Ye, and S. Zhang, "Semidefinite relaxation of quadratic optimization problems," *IEEE Signal Processing Magazine*, vol. 27, no. 3, pp. 20–34, 2010.

[50] G. H. Hardy, J. E. Littlewood, and G. Pólya, *Inequalities*. Cambridge university press, 1952.

Prabhat Raj Gautam received the Master of Technology degree in communications engineering from Indian Institute of Technology (IIT) Delhi, India in 2015, and the Ph.D. degree in Electronic and Electrical Engineering from University of Leeds, UK in 2023. He is currently a Research Fellow at the Department of Computing, Imperial College London. His research focuses on wireless communications, with particular interest in millimeter-wave communications, reconfigurable intelligent surface (RIS)-enhanced communications, and integrated sensing and communication (ISAC). He received the Best Student Paper Award at the International Symposium on Wireless Personal Multimedia Communications (WPMC2019), in 2019. He was also awarded the F.W. Carter Prize for the best Ph.D. thesis at the University of Leeds.

Julie A. McCann is currently a Professor in computer systems with the Imperial College London, also the Co-Director of the School of Convergence Science in Security, Space and Telecoms, and the Director of the National CHEDDAR Communications Research Hub. She leads the Adaptive Emergent Systems Engineering Research (AESE) Research Group, Critical Ecosystems Lead for the Alan Turing Institute, and Imperial PI on the EPSRC Programme Grant Science for Sensor Systems Software. She is an elected member of the Council of Computer Science Professors and Heads of Computing and was elected to the Membership Committee of the UKCRC, she holds the 2018 UKRI Suffrage Science Award for Computing and Mathematics, President's Medal for Research Excellence 2020. She is a fellow of the BCS and Chartered Engineer.